

Quantum transport in mesoscopic ring structures: Effects of impurities, long-range hopping and interactions

Santanu K. Maiti^{1, *}

¹*Physics and Applied Mathematics Unit, Indian Statistical Institute,
203 Barrackpore Trunk Road, Kolkata-700 108, India*

In the present review we make a comprehensive analysis of our understanding on electron transport in mesoscopic single-channel rings and multi-channel cylinders within a tight-binding framework. A spectacular mesoscopic phenomenon where a non-decaying current circulates in a small conducting loop is observed upon the application of an Aharonov-Bohm flux ϕ . To understand its behavior one has to focus attention on the interplay of quantum phase coherence, electron-electron correlation and disorder. This is a highly challenging problem and here we address it for some simple loop geometries with their detailed energy band structures to get an entire picture at the microscopic level. The behavior of low-field magnetic response of persistent current and its temperature dependence are also discussed.

PACS numbers: 73.23.-b, 73.23.Ra, 71.27.+a, 73.63.Nm, 75.20.-g, 68.65.-k

I. INTRODUCTION

An emerging tendency in modern material science is to propose and investigate systems containing smaller and smaller structures. These smaller structures approach the so-called mesoscopic or nanoscopic regimes in which quantum effects become much more significant for the behavior of these materials. This situates mesoscopic physics at the interface of statistical and quantum pictures. The mesoscopic systems are very much smaller than the large-scale objects and they often have unusual physical and chemical properties. The study of such systems provides a clear understanding of the behavior of a material as it goes from a few atoms to large visible and tangible objects.

A. The mesoscopic regime

The mesoscopic scale refers to the length scale at which one can reasonably describe the properties of a material or a phenomenon without discussing the behavior of the individual atoms. For solids it is typically a few to ten nanometers and involves averaging over a few thousand atoms or molecules. In this scale the expected fluctuations of the averaged physical quantities due to the motion and behavior of individual particles can be reduced below some desirable threshold (often to a few percent) and it must be rigorously established within the context of any particular problem. In the mesoscopic regime, behavior of a system is considerably influenced by quantum interference of electronic wave functions. The quantum phase coherence, essential for the appearance of interference effects, is preserved only during a finite time τ_ϕ the so-called phase coherence time. In electronic conductors, finite phase coherence time corresponds to a phase coherence length L_ϕ over which electrons can travel before their phase coherence gets lost. Mesoscopic quantum effects appear when the typical time or length scales of

the system are smaller than the phase coherence time or length. In many cases this means that the relevant system size L must be smaller than the phase coherence length L_ϕ . For an electron, the phase coherence time/length is limited by electron-electron and electron-phonon scattering. These processes are important at high temperatures, but both are suppressed at low temperatures implying that the phase coherence time/length is strongly material and temperature dependent.

The mesoscopic regime is therefore characterized by small time and/or length scales and low temperatures. When temperature is lowered, the phase coherence time/length increases (by a factor T^{-1}), and the mesoscopic regime gets extended. At sub-Kelvin temperatures, the time and the length scales in semiconductor samples are of the order of picoseconds and micrometers, respectively.

B. Some extraordinary mesoscopic phenomena

The samples like quantum dots, quantum wires, two-dimensional electron gases in semiconductor heterostructures, etc., exhibit many alluring physical properties. Here we briefly describe some spectacular effects that appear in such systems as a consequence of quantum phase coherence of electronic wave functions.

1. Aharonov-Bohm oscillation

One of the most notable consequences of quantum phase coherence is the Aharonov-Bohm (AB) oscillation in conductance of normal metal mesoscopic rings. At low temperatures superposition of electronic waves propagating along two arms of a ring becomes important. The pioneering experiment on AB effect was done on a ring-shaped resistor made from a 38 nm film of polycrystalline gold. The diameter of it is 820 nm and the thickness of the wire is 40 nm¹. The conductance shows oscillating

behavior as a function of magnetic flux enclosed by the ring with $h/|e|$ periodicity²:

$$g = g_0 + \hat{g} \cos \left[\frac{|e|BS}{\hbar} + \bar{\phi} \right] \quad (1)$$

where S is the area enclosed by the ring and B is the applied magnetic field perpendicular to the ring plane.

2. Integer quantum Hall effect

One of the most stunning discoveries of 1980s was the integer quantum Hall effect (IQHE)³ as a result of quantum phase coherence of electronic wave functions in two-dimensional electron gas (2DEG) systems. In the Hall measurement, one drives a current along a conductor (2DEG), and measures the longitudinal voltage V_x and transverse Hall voltage V_H as a function of magnetic field B applied perpendicular to the plane of the conductor. According to the classical Drude formula, the Hall resistance R_H varies linearly with the field strength B , while the longitudinal resistance R_x gets unaffected by this field. This behavior holds true only when magnetic field is too weak. In strong magnetic field and at low temperatures, one gets completely different behavior which cannot be explained by the classical Drude model. At high field longitudinal resistance shows oscillatory behavior, while Hall resistance exhibits step-like nature with sharp plateaus. The values of R_H on these plateaus are given by h/ne^2 , where n is an integer with values 1, 2, 3, ... and it turns out that these values of R_H are highly reproducible with a great precision and are also very robust so that they are often used as resistance standard. The integer quantum Hall effect is a purely quantum mechanical phenomenon due to the formation of the Landau levels and many good reviews on IQHE are available in literature⁴⁻⁶.

3. Fractional quantum Hall effect

At extremely high magnetic fields and low temperatures, a 2DEG provides additional plateaus in the Hall resistance at fractional filling factors and this phenomenon was discovered in 1982⁷. Unlike the integer quantum Hall effect, it has been observed that the Coulomb correlation between the electrons becomes important for the interpretation of the fractional quantum Hall effect and the presence of fractional filling has been traced back to the existence of correlated collective quasi-particle excitations⁸. This phenomenon has been reviewed in detail by Chakraborty *et al.*⁵.

4. Conductance fluctuations and quantization

In the mesoscopic regime, conductance of disordered wires exhibits pronounced fluctuations as a function of

external parameters, like magnetic field or Fermi energy. These fluctuations were observed⁹ only at very low temperatures which are perfectly reproducible and represent a fingerprint of the quantum effects in samples. The fluctuations appear due to the interference of electronic wave functions corresponding to different pathways that the electrons can take when traversing through a system. The most significant feature of this conductance fluctuations is that their typical amplitude is universal in the diffusive regime¹⁰. The fluctuations are always of the order of the conductance quantum e^2/h and depend only on the basic symmetries of the system¹¹.

The conductance of ballistic quantum point contacts was found^{12,13} to be quantized in units of $2e^2/h$ and a recent experiment¹⁴ demonstrates that the conductance quantization can be observed even in an extremely simple setup. A quantum point contact is a very narrow link between two conducting materials formed by imposing a narrow constriction into them. With the decrease of the width (W) of constriction it has been observed that conductance goes down in quantized steps. This is due to the fact that although the width of the constriction changes continuously, the number of sub-bands or transverse modes (M) changes in discrete steps. This discreteness is not evident if the constriction is several thousands of wavelengths wide, since then a very small fractional change in W changes M by many integers.

5. Persistent current

The physics of small conducting rings provides an excellent testing ground for many ideas of fundamental physics. In thermodynamic equilibrium, a small metallic ring threaded by an AB flux ϕ supports a current that does not decay dissipatively even at non-zero temperature. It is the well-known phenomenon of persistent current in mesoscopic normal metal rings. This is a purely quantum mechanical effect and gives a lucid exposition of the AB effect¹⁵. The possibility of persistent current was predicted in the very early days of quantum mechanics by Hund¹⁶, but their experimental evidences came much later only after realization of the mesoscopic systems. In 1983, Büttiker *et al.*¹⁷ predicted theoretically that persistent current can exist in mesoscopic normal metal rings threaded by a magnetic flux even in the presence of impurity. This quantum phenomenon has been verified experimentally in a pioneering work of Levy *et al.*¹⁸ and later the existence of persistent current has been further confirmed by several other nice experiments¹⁹⁻²⁵. Though much efforts have been paid to study persistent current both experimentally¹⁸⁻²⁵ as well as theoretically²⁶⁻⁵¹, yet several anomalies still exist between the theory and experiment, and the full knowledge about it in this scale is not well rooted even today. One of the important controversies is related to the concrete prediction of persistent current amplitudes in mesoscopic rings. The results of the single loop experiments are somewhat different from

those for the ensemble of isolated loops. Levy *et al.*¹⁸ found oscillations with period $\phi_0/2$ rather than ϕ_0 in an ensemble of 10^7 independent Cu rings. Similar $\phi_0/2$ oscillations were also reported for an ensemble of disconnected 10^5 Ag rings¹⁹ as well as for an array of 10^5 isolated GaAs-AlGaAs rings²⁰. In a recent experiment, Jariwala *et al.*²¹ obtained both ϕ_0 and $\phi_0/2$ periodic persistent currents in an array of thirty diffusive mesoscopic Au rings. Persistent currents with expected ϕ_0 periodicity have been observed in isolated single Au rings²² and in a GaAs-AlGaAs ring²³. Except for the case of nearly ballistic GaAs-AlGaAs ring²³, all the measured currents are in general one or two orders of magnitude larger than those expected from the theory.

Free electron theory predicts that at absolute zero temperature ($T = 0\text{K}$), an ordered one-dimensional (1D) metallic ring threaded by a magnetic flux ϕ supports persistent current with maximum amplitude $I_0 = ev_F/L$, where v_F is the Fermi velocity and L is the circumference of the ring. Metals are intrinsically disordered which tends to decrease persistent current, and the calculations show that the disorder-averaged current $\langle I \rangle$ crucially depends on the choice of the ensemble²⁸⁻³⁰. The magnitude of the current $\langle I^2 \rangle^{1/2}$ is however insensitive to averaging issues, and is of the order of $I_0 l/L$, l being the elastic mean free path of electrons. This expression remains valid even if one takes into account the finite width of the ring by adding contributions from transverse channels, since disorder leads to a compensation between the channels^{28,29}. However, the measurements on an ensemble of 10^7 Cu rings¹⁸ reported a diamagnetic persistent current of average amplitude $3 \times 10^{-3} ev_F/L$ with half a flux-quantum periodicity. Such $\phi_0/2$ oscillations with diamagnetic response were also found in other persistent current experiments consisting of ensemble of isolated rings^{19,20}.

Measurements on single isolated mesoscopic rings on the other hand detected ϕ_0 -periodic persistent currents with amplitudes of the order of $I_0 \sim ev_F/L$, (closed to the value for an ordered ring). Theory and experiment²³ seem to agree only when *disorder is weak*. In another recent experiment Bluhm *et al.*²⁴ have measured magnetic response of 33 individual cold mesoscopic gold rings, one ring at a time, using a scanning SQUID technique. They have measured h/e component and anticipated that the measured current amplitude agrees quite well with theory²⁷ in a single ballistic ring²³ and an ensemble of 16 nearly ballistic rings⁵². However, the amplitudes of the currents in single-isolated-diffusive gold rings²² were two orders of magnitude larger than the theoretical estimates. This discrepancy instituted intense theoretical activity, and it is generally believed that the electron-electron correlation plays an important role in the disordered diffusive rings^{37,53,54}. An explanation based on the perturbative calculation in presence of interaction and disorder has been proposed and it seems to give a quantitative estimate closer to the experimental results, but still it is less than the measured currents by an order of magni-

tude, and the interaction parameter used in the theory is not well understood physically.

The other paramount debate arises in determining the sign of low-field currents and still it is an unresolved issue between theoretical and experimental results. In an experiment Levy *et al.*¹⁸ have shown diamagnetic nature of the measured currents at low-field limit. Jariwala *et al.*²¹ have predicted diamagnetic persistent current in their experiment and similar diamagnetic response in the vicinity of zero-field limit were also supported in an experiment done by Deblock¹⁹ *et al.* on Ag rings. In other experiment Chandrasekhar *et al.*²² have obtained paramagnetic response near zero-field limit. Yu and Fowler⁵⁵ have shown both diamagnetic and paramagnetic responses in mesoscopic Hubbard rings. Though in a theoretical work Cheung *et al.*²⁸ have revealed that the direction of current is random depending on total number of electrons in the system and the specific realization of random potentials. Hence, prediction of the sign of low-field currents is still an open challenge and further studies on persistent current in mesoscopic systems are needed to remove the existing controversies.

The main motivation of the present review is to address some important aspects of persistent current and low-field magnetic susceptibility in single-channel mesoscopic rings and multi-channel cylinders which are quite challenging from the standpoint of theoretical as well as experimental research. A brief layout of the presentation is as follows.

Following a short description of some extraordinary mesoscopic phenomena (Section I), in Section II we study the phenomenon of persistent current in ordered and disordered rings within a non-interacting electron picture. The effects of electron-electron interaction on persistent current are explored in Section III. In Section IV, we show that the contributions of higher order hopping integrals are quite important for the enhancement of persistent current in disordered mesoscopic rings. The sign of persistent current in the limit $\phi \rightarrow 0$, determined by calculating magnetic susceptibility, and its temperature dependence are analyzed in Section V. Finally, we conclude in Section VI.

Throughout the review we choose $c = e = h = 1$ for numerical calculations.

II. PERSISTENT CURRENT IN NON-INTERACTING SINGLE-CHANNEL AND MULTI-CHANNEL MESOSCOPIC RINGS

Our aim of this section is to inspect the behavior of persistent current in some small non-superconducting loops threaded by a magnetic flux ϕ . A conducting ring, penetrated by a magnetic flux ϕ , carries an equilibrium current in its ground state that *persistent* (does not decay) in time. An electrically charged particle moving around the ring but not entering the region of magnetic flux, feels no (classical) force during its motion. However, the mag-

netic vector potential \vec{A} , associated with magnetic field \vec{B} through the relation $\vec{B} = \vec{\nabla} \times \vec{A}$, affects the quantum state of the particle by changing the phase of its wave function. As a consequence, both thermodynamic and kinetic properties oscillate with flux ϕ . Here, we present some analytical and numerical results to study the characteristic properties of persistent current I in mesoscopic rings as functions of AB flux ϕ , system size L , total number of electrons N_e , chemical potential μ and disorder strength W .

A. General formulation of persistent current

In this sub-section we illustrate the theoretical formulation of persistent current appears in a metallic ring in presence of an AB flux ϕ . Let us begin with the model

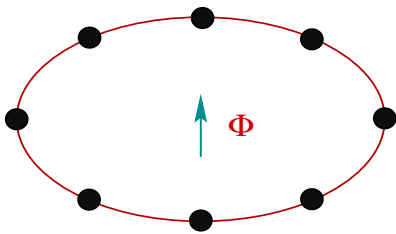


FIG. 1: (Color online). One-dimensional ring threaded by an AB flux ϕ . Filled circles correspond to the positions of the atomic sites. A persistent current I is established in the ring.

quantum system given in Fig. 1. The electric field \mathcal{E} associated with magnetic field B in the ring can be expressed through the relation (Faraday's law),

$$\vec{\nabla} \times \vec{\mathcal{E}} = -\frac{1}{c} \frac{\partial \vec{B}}{\partial t}. \quad (2)$$

This relation enables us to determine the electric field \mathcal{E} from the following expressions:

$$\oint_S (\vec{\nabla} \times \vec{\mathcal{E}}) \cdot d\vec{S} = -\frac{1}{c} \oint_S \frac{\partial \vec{B}}{\partial t} \cdot d\vec{S} = -\frac{1}{c} \frac{\partial}{\partial t} \oint_S \vec{B} \cdot d\vec{S} = -\frac{1}{c} \frac{\partial \phi}{\partial t} \quad (3)$$

where, S is the area enclosed by the ring. From Stoke's theorem we get,

$$\oint_{loop} \vec{\mathcal{E}} \cdot d\vec{l} = -\frac{1}{c} \frac{\partial \phi}{\partial t} \quad (4)$$

and thus the electric field can be written in terms of the time variation of magnetic flux ϕ as,

$$\mathcal{E} = -\frac{1}{2\pi r c} \frac{\partial \phi}{\partial t} \quad (5)$$

where r is the radius of the ring. Therefore, the force experienced by an electron in the ring becomes,

$$F = -\frac{e}{2\pi r c} \frac{\partial \phi}{\partial t} \quad (6)$$

and the change in energy or work done for a small displacement Δs is,

$$\Delta E = \Delta W = \vec{F} \cdot \vec{\Delta s} = -\frac{e}{2\pi r c} \frac{\Delta \phi}{\Delta t} \Delta s = -\frac{e}{2\pi r c} \Delta \phi \left(\frac{\Delta s}{\Delta t} \right). \quad (7)$$

The velocity of the electron in the ring is thus written as,

$$v = \frac{\Delta s}{\Delta t} = -\frac{2\pi r c}{e} \left(\frac{\Delta E}{\Delta \phi} \right) \quad (8)$$

and accordingly, the persistent current developed in the ring gets the form,

$$I = ef = \frac{ev}{2\pi r} = -c \left(\frac{\Delta E}{\Delta \phi} \right). \quad (9)$$

This is the most general expression of persistent current in a loop geometry threaded by an AB flux ϕ and it shows that the current can be obtained by taking the first order derivative of energy with respect to flux ϕ .

B. Non-interacting one-channel rings

This sub-section focuses attention on the behavior of persistent current in one-channel rings⁵⁶ where the ring are described by a simple non-interacting tight-binding (TB) framework. The TB Hamiltonian for a N -site ring threaded by a magnetic flux ϕ (measured in unit of the elementary flux quantum $\phi_0 = ch/e$) reads,

$$H = \sum_i \epsilon_i c_i^\dagger c_i + \sum_{\langle ij \rangle} t \left[e^{i\theta} c_i^\dagger c_j + e^{-i\theta} c_j^\dagger c_i \right] \quad (10)$$

where, c_i^\dagger (c_i) corresponds to the creation (annihilation) operator of an electron at the site i , t gives the nearest-neighbor hopping integral, ϵ_i is the on-site energy and $\theta = 2\pi\phi/N$ is the phase factor due to the flux ϕ threaded by the ring. The magnetic flux ϕ enters explicitly into the above Hamiltonian (Eq. 10), and the wave functions satisfy the periodic boundary condition which is equivalent to consider the above Hamiltonian at zero flux with the flux-modified boundary conditions:

$$\begin{aligned} \psi|_{x=L} &= \exp\left[\frac{2\pi i\phi}{\phi_0}\right] \psi|_{x=0} \\ \frac{d\psi}{dx}\Big|_{x=L} &= \exp\left[\frac{2\pi i\phi}{\phi_0}\right] \frac{d\psi}{dx}\Big|_{x=0} \end{aligned} \quad (11)$$

Here, x varies between 0 to L and is expressed as $x = L\theta'/2\pi$, where θ' is the azimuthal angle, the spatial degrees of freedom of an electron in the ring.

1. Impurity free rings

In order to reveal the basic properties of persistent current, let us start our discussion with the energy band

structure of a simplest possible system which is the case of impurity free non-interacting electron model.

Energy spectra: For a perfect ring, setting $\epsilon_i = 0$ we get the energy of n th eigenstate as,

$$E_n(\phi) = 2t \cos \left[\frac{2\pi}{N} \left(n + \frac{\phi}{\phi_0} \right) \right] \quad (12)$$

where, $n = 0, \pm 1, \pm 2, \dots$. In Fig. 2, we present energy-flux (E - ϕ) characteristics of a perfect ring considering the system size $N = 10$. It shows that the energy levels vary periodically with ϕ providing ϕ_0 flux-quantum periodicity. At an integer or half-integer flux quantum, each of

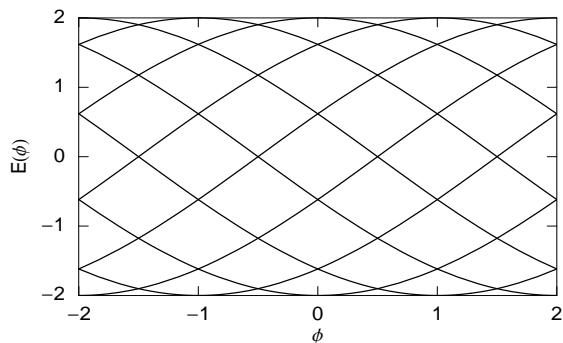


FIG. 2: Energy levels as a function of flux ϕ for a one-dimensional impurity-free ring when N is set at 10.

the energy levels has an extremum i.e., either a maximum or a minimum, and therefore, at these values of ϕ current should disappear. Below, we discuss the current-flux (I - ϕ) characteristics for two different cases. In one case we take the rings with fixed number of electrons N_e , and in the other case the rings have some constant chemical potential μ .

Persistent current: rings with fixed N_e : The current carried by the n th energy eigenstate, whose energy is given by Eq. 12, can be obtained through the relation,

$$I_n(\phi) = \left(\frac{4\pi t}{N\phi_0} \right) \sin \left[\frac{2\pi}{N} \left(n + \frac{\phi}{\phi_0} \right) \right]. \quad (13)$$

At absolute zero temperature ($T = 0\text{K}$), total persistent current is determined by taking the sum of individual contributions from the lowest N_e energy levels. The variation of persistent current as a function of flux ϕ is presented in Fig. 3, where (a) corresponds to the ring with odd N_e , while the results for even N_e are shown in (b). From the spectra we observe that the current exhibits a saw-tooth like behavior with sharp transitions at half-integer and integer flux quanta for the rings having odd and even N_e , respectively. For all these cases, current varies periodically with ϕ providing ϕ_0 periodicity.

Persistent current: rings with fixed μ : When the rings are characterized with fixed chemical potential μ , instead of N_e , total current at $T = 0\text{K}$ will be obtained by adding

all individual contributions from the energy levels having energies less than or equal to μ . As the chemical potential is fixed, total number of electrons varies as a

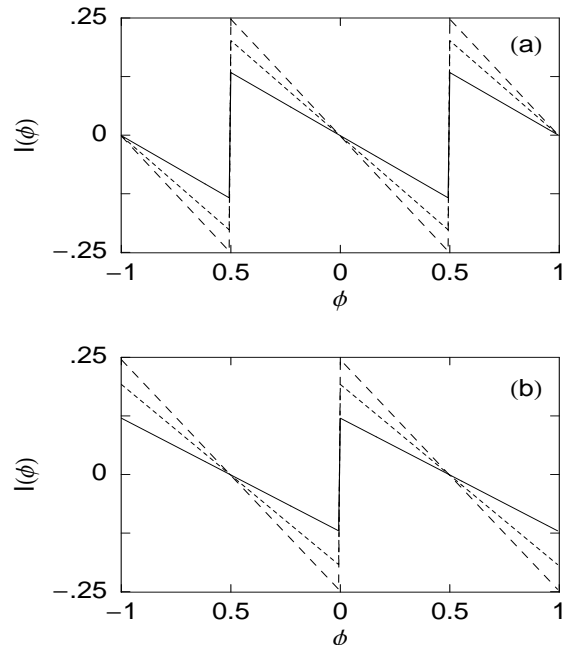


FIG. 3: Current-flux characteristics for an ordered one-channel mesoscopic ring when N is fixed at 50. The solid, dotted and dashed curves in (a) correspond to $N_e = 9, 15$ and 23, respectively, while in (b) they represent $N_e = 8, 14$ and 22, respectively.

function of AB flux ϕ except for some typical choices of μ , where the rings contain fixed number of electrons. In Fig. 4, we illustrate current-flux characteristics for a single-channel mesoscopic ring, described with constant μ , when the ring is free from impurities. Here we set $N = 100$. Several kink-like structure appears at different values of flux ϕ , associated with the choice of μ which is clearly observed from the I - ϕ spectra (Fig. 4). All these currents oscillate with ϕ exhibiting ϕ_0 periodicity.

2. Rings with impurity

Metals are intrinsically disordered which tends to decrease persistent current due to the localization effect⁵⁷ of energy eigenstates. To address the role of impurities on persistent current now we analyze the behavior of current-flux characteristics together with energy band structure of some typical mesoscopic rings in presence of disorder.

Energy spectra: In presence of impurity in a ring, finite gaps open between the energy levels at the points of intersection, like as energy gaps generated in the band structure problem. All these energy levels vary continuously

with flux ϕ and no crossing between the neighboring levels takes place through the energy band window. In Fig. 5 we present the energy band structure of a single-channel ring in presence of diagonal disorder setting $N = 10$. The impurities in the ring are introduced by selecting

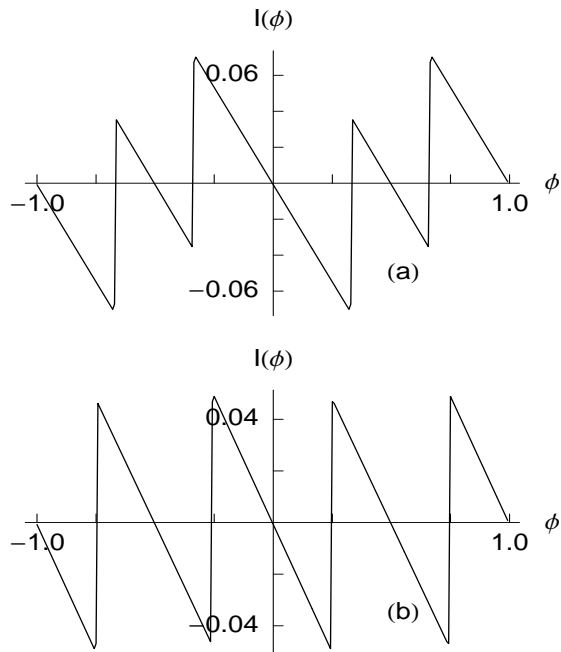


FIG. 4: Persistent current as a function of ϕ for an ordered mesoscopic ring, where (a) $\mu = -1$ and (b) $\mu = -1.25$. Here we fix $N = 100$.

the on-site energies, ϵ_i , randomly from a “Box” distribution function of width $W = 1$. In presence of impurity all

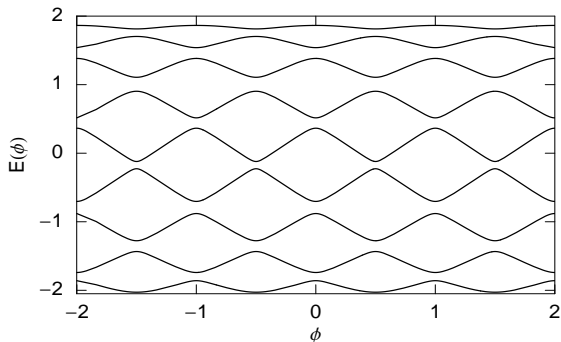


FIG. 5: Electron energy levels as a function of the flux ϕ for a one-channel ring ($N = 10$) in the presence of impurity with strength $W = 1$.

the degeneracies get removed and energy levels oscillates continuously, without exhibiting any crossing, result a smooth variation of persistent current which can be followed from the forthcoming sub-sections.

Persistent current: rings with constant N_e : The characteristic behavior of persistent current in presence of dis-

order is illustrated in Fig. 6 where we set the disorder strength $W = 1$. The results are shown for a 50-site single-channel ring, where (a) corresponds to the results for odd N_e and the results for even N_e are given in (b). From the spectra it is observed that the current varies

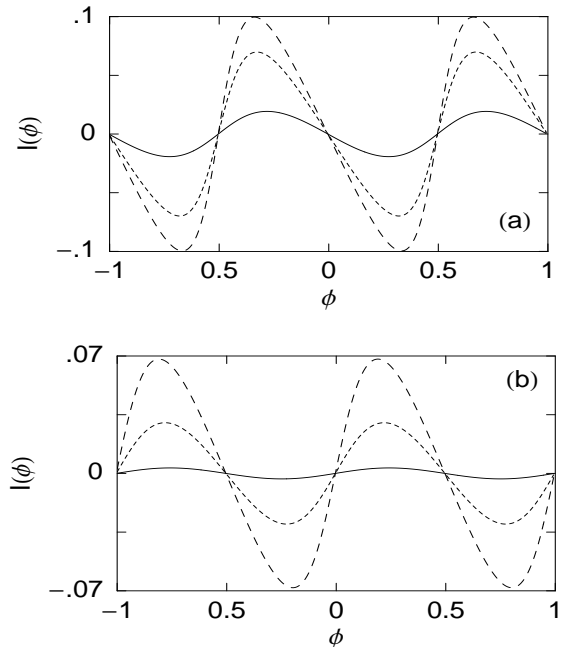


FIG. 6: Persistent current as a function of flux ϕ for a disordered ring described with constant N_e . The solid, dotted and dashed line in (a) correspond to $N_e = 9, 15$ and 23 , respectively, while in (b) they represent $N_e = 8, 14$ and 22 , respectively. Here we set $N = 50$ and $W = 1$.

continuously as a function of ϕ with much reduced amplitude compared to the impurity-free case (see Fig. 3). The smooth variation of persistent current is clearly followed from the energy band spectrum since energy levels become continuous as long as the impurities are introduced in the ring. On the other hand, the suppression of current amplitudes is solely due to the localization effect of the energy eigenstates in the presence of impurity. Here all these results are described for some typical disordered configurations, and in fact, we examine that the qualitative behavior of the persistent currents does not depend on the specific realization of disordered configurations. This is a generic feature of persistent current for any one-channel non-interacting rings in presence of impurity those are described with constant N_e .

Persistent current: rings with constant μ : The situation is somewhat interesting when we fix μ instead of N_e to characterize persistent current in a disordered mesoscopic ring. As representative example, in Fig. 7 we present the results for a disordered ring, where we fix $\mu = -1$ in (a) and in (b) μ is set equal to -1.5 . Interestingly, it is observed that depending on the choice of μ persistent current can exhibits a continuous-like or a kink-like vari-

ation with flux ϕ . In all these cases current oscillates periodically with ϕ showing ϕ_0 flux-quantum periodicity.

C. Non-interacting multi-channel rings

In this sub-section we focus our attention on magneto-transport of non-interacting electrons in multi-channel

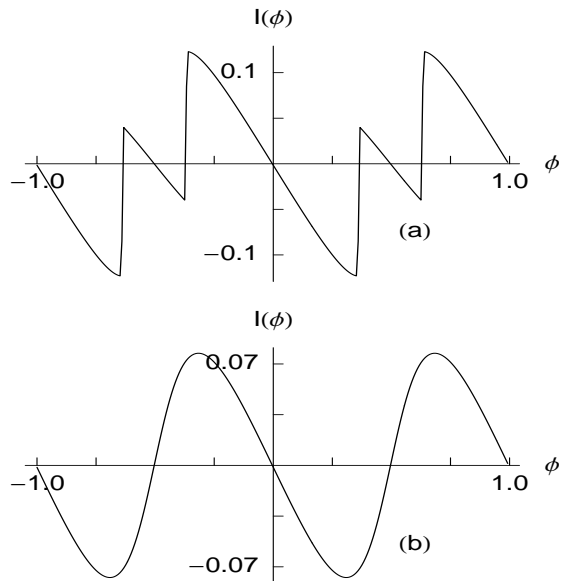


FIG. 7: Persistent current as a function of flux ϕ for a disordered ring, where (a) $\mu = -1$ and (b) $\mu = -1.25$. The ring size and impurity strength are the same as in Fig. 6.

mesoscopic rings⁵⁶ studied within a simple one-band tight-binding Hamiltonian. A schematic view of such a

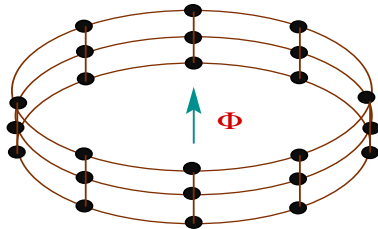


FIG. 8: (Color online). Schematic view of a multi-channel cylinder threaded by a magnetic flux ϕ . Filled circles correspond to the atomic sites in the cylinder.

multi-channel ring geometry threaded by an AB flux ϕ is shown in Fig. 8. Considering the lattice spacing both in the longitudinal and transverse directions are identical i.e., the surface of the cylinder forms a square lattice, we can write the Hamiltonian of the system by the TB formulation as,

$$H = \sum_x \epsilon_x c_x^\dagger c_x + \sum_{\langle xx' \rangle} \left[t_{xx'} e^{i\theta_{xx'}} c_x^\dagger c_{x'} + t_{xx'} e^{-i\theta_{xx'}} c_{x'}^\dagger c_x \right] \quad (14)$$

where, ϵ_x is the on-site energy of the lattice point x of coordinate, say, (i, j) . $t_{xx'}$ is the hopping strength between the lattice points x and x' and $\theta_{xx'}$ is the phase factor acquired by an electron due to the longitudinal hopping in presence of AB flux ϕ . The study of persistent currents in such multi-channel systems becomes much more relevant compared to strictly one-dimensional rings (see Fig. 1), where we get only one channel that carries current, since most of the conventional experiments are performed in rings with finite width. Here, we will describe the characteristic properties of persistent current together with energy band spectrum for some non-interacting multi-channel rings concerning the dependence of the current on total number of electrons N_e , chemical potential μ , strength of disorder W and number of channels.

1. Energy band structure

To elucidate the nature of persistent current in mesoscopic multi-channel systems, let us first describe the energy-flux characteristics of a small cylindrical system

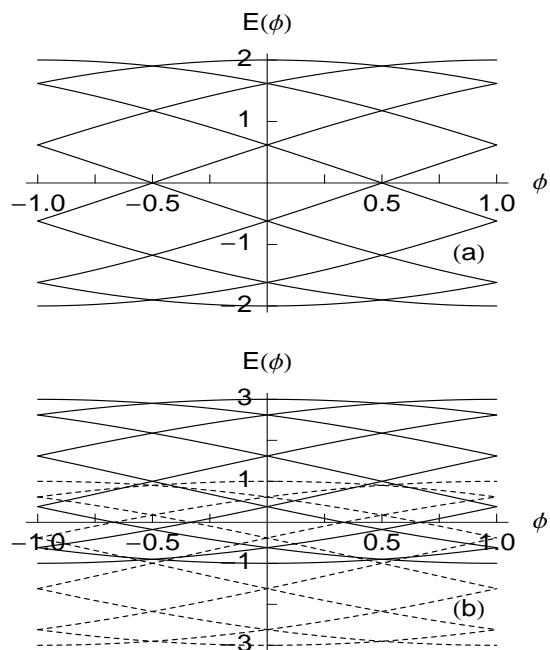


FIG. 9: Energy levels as a function of magnetic flux ϕ , for (a) a perfect ring (one layer) with $N = 10$ and (b) a perfect cylinder having two identical rings taking $N = 10$ in each of these two rings.

that threads a magnetic flux ϕ . In order to have a deeper insight to the problem we begin our discussion with the simplest possible system which can be calculated analytically. This is the case of a two-layer impurity free cylinder threaded by a magnetic flux ϕ . This cylindrical system can be treated as two one-channel rings placed one above the other and they are connected by some vertical bonds

(like as in Fig. 8). For a strictly one-dimensional ring i.e., for one layer the energy of n th eigenstate is expressed in the form $E_n(\phi) = 2t \cos \left[\frac{2\pi}{N} \left(n + \frac{\phi}{\phi_0} \right) \right]$ (see Eq. 12), where $n = 0, \pm 1, \pm 2, \dots$. Here t is the nearest-neighbor hopping strength and N is the total number of lattice points in the ring. The behavior of such energy levels is shown in Fig. 9(a), where we choose $N = 10$. This spectrum indicates that the energy levels are bounded within the range -2 to 2 in the scale of t and the crossing of the energy levels (flux points where energy levels have degeneracy) occurs at half-integer or integer multiples of ϕ_0 . Now as we add another ring with the previous one-dimensional ring and connect it by N vertical bonds it becomes a regular cylinder with two identical layers. For such a system, two different energy bands are obtained, each of which contains N number of energy levels and they are respectively expressed in the form, $E_{1n}(\phi) = -t + 2t \cos \left[\frac{2\pi}{N} \left(n + \frac{\phi}{\phi_0} \right) \right]$ and $E_{2n}(\phi) = -t + 2t \cos \left[\frac{2\pi}{N} \left(n + \frac{\phi}{\phi_0} \right) \right]$, where the symbol n corresponds to the same meaning as above and t is the nearest-neighbor hopping strength which is identical both for the longitudinal and transverse directions. In Fig. 9(b), we show the energy levels of a small impurity-free cylinder considering $N = 10$, where the solid and dotted line represent the energy levels in two separate energy bands, respectively. These two different energy bands are bounded respectively in the range -1 to 3 and -3 to 1 in the scale of t . Accordingly, an overlap energy region appears for these two energy bands within the range -1 to 1 , as shown in Fig. 9(b). In this overlap region, energy levels cross each other at several other flux points in addition to the half-integer and integer multiples of ϕ_0 which result different characteristic features of persistent current. For cylinders with more than two layers, we get more energy bands like above and therefore several other overlap energy regions appear in energy band spectrum.

In presence of impurity in multi-channel cylinders, gaps open at crossing points of energy levels and they provide a continuous-like variation with AB flux ϕ , similar to the case of conventional one-dimensional rings with impurities (Fig. 5). In all these perfect and disordered multi-channel cylinders, energy levels vary periodically with period ϕ_0 .

Below, we will investigate the behavior of persistent current in small cylindrical systems and we believe that the results might be quite helpful to explain characteristic properties of persistent current in larger system sizes, even in more complex geometries.

2. Persistent current

Perfect cylinders: Here we describe the phenomenon of persistent current for some impurity-free multi-channel systems of cylindrical geometry containing two layers

concerning the dependence of current on total number of electrons N_e and chemical potential μ . As illustrative example, in Fig. 10 we show the variation of persistent current as a function of AB flux ϕ for an ordered cylinder taking $N = 100$ in each of these two layers. The first column corresponds to the case where the cylinder is characterized with constant N_e , while the second column represents the results where we fix μ instead of N_e . To reveal the effect of energy overlap region on persistent current here we present our results for three different values of N_e . Figures 10(a) and (c) correspond to

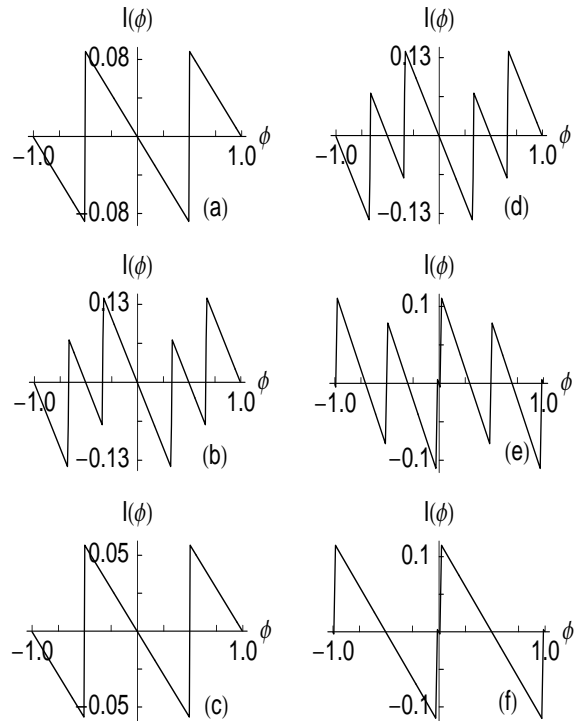


FIG. 10: Persistent current as a function of AB flux ϕ for an ordered mesoscopic cylinder with two layers in which each layer contains 100 atomic sites. The first column corresponds to the results for constant N_e , where (a) $N_e = 25$, (b) $N_e = 100$ and (c) $N_e = 185$, while the second column describes the results for fixed μ , where (d) $\mu = 0$, (e) $\mu = -0.5$ and (f) $\mu = -1.5$.

the currents when $N_e = 25$ (low) and $N_e = 185$ (high), respectively, while the current for the intermediate value of N_e ($N_e = 100$) is shown in Fig. 10(b). Both for the low and high values of N_e , we notice that the current gets saw-tooth like nature with sharp transitions only at half-integer multiples of ϕ_0 , similar to that of conventional one-channel impurity-free rings with odd N_e (Fig. 3(a)). This feature can be explained as follows. When N_e is set at 25, the net current is available by taking the contributions from lowest 25 energy levels those lie well below the energy overlap region. Now, away from this overlap region, the energy levels behave exactly the same way with perfectly single-channel rings, which results a sim-

ilar kind of saw-tooth shape as obtained in one-channel rings. On the other hand, when the filling factor N_e is fixed at 185 the situation is somewhat different than the earlier one. To obtain net current for this case we cross the overlap energy region since the highest energy level that contributes current lies far above this overlap region and the net contribution to the current from the energy levels within this overlap region vanishes and therefore no new feature appears in persistent current compared to the system with $N_e = 25$. Finally, we see that for the intermediate value of N_e ($N_e = 100$) persistent current gives some additional kink-like structures across $\phi = \pm 0.5$. These kinks are due to the different con-

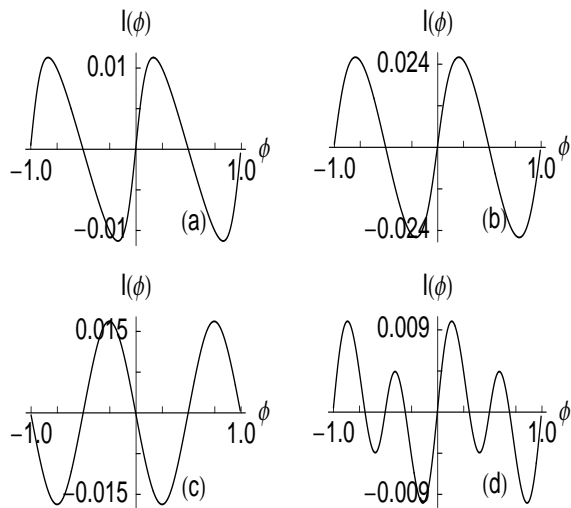


FIG. 11: Current-flux characteristics for the disordered ($W = 1$) cylinders with two layers taking $N = 100$ in each layer. The results for the fixed N_e are plotted in the first column, where (a) $N_e = 50$ and (b) $N_e = 100$, while the results for the constant μ are plotted in the second column, where (c) $\mu = 0$ and (d) $\mu = -0.5$.

tributions of energy levels in the overlap energy region, since in this region energy levels have more degeneracies at different flux points in addition to the half-integer and integer multiples of ϕ_0 . For other multi-channel systems with more than two layers, additional kinks may appear in persistent current at different values of ϕ depending on the choice of N_e and number of layers.

In this cylindrical system where we fix chemical potential μ instead N_e , different kink-like structures in persistent current are also appeared as visible from our results shown in the second column of Fig. 10. All these cases current exhibits ϕ_0 flux-quantum periodicity.

Disordered cylinders: At the end of this sub-section, we describe the effect of impurities on persistent current in a multi-channel system. The results shown in Fig. 11 and they are computed for the same system size as taken above. The impurities are introduced by selecting the site energies (ϵ_x) randomly from a “Box” distribution function of width $W = 1$. All these numerical results

are performed for different isolated disordered configurations. The results for constant N_e are shown in the first column, while in the second column the results for fixed μ are presented. In all these cases persistent current varies continuously, without providing any kink-like structure, as a function of flux ϕ exhibiting ϕ_0 flux-quantum periodicity. Another significant point observed from Figs. 11(a) and (b) is that the slope of the current in zero-field limit ($\phi \rightarrow 0$) changes in opposite direction though in these two cases the cylinder contains even number of electrons. This emphasizes the signature of random sign of low-field currents in multi-channel systems. The detailed description of low-field magnetic response will be available in Section V.

Thus we can summarize that the behavior of persistent current in multi-channel systems strongly depends on total number of electrons N_e , chemical potential μ , total number of channels and disordered configurations.

III. EFFECT OF ELECTRON-ELECTRON CORRELATION ON PERSISTENT CURRENT IN ONE-CHANNEL RINGS

The phenomenon of persistent current in small conducting ring threaded by a magnetic flux ϕ was predicted in the pioneering work of Büttiker, Imry and Landauer¹⁷, and since then it has been discussed in several theoretical papers^{26–38}. Although this phenomenon is thought to be qualitatively understood within the framework of one-electron picture^{27–36}, but it fails to explain many experimental results^{18–23}. A typical example of such discrepancy between theory and experiment is that the amplitudes of measured persistent currents are orders of magnitude larger than theoretical predictions. It is generally believed that electron-electron correlation and disorder have major role on the enhancement of persistent current, but no consensus has yet been reached. Another important controversial issue is that, experimentally both ϕ_0 and $\phi_0/2$ periodicities have been observed and it is also found that the $\phi_0/2$ oscillations near zero magnetic flux exhibit diamagnetic response. The explanation of these results in terms of the ensemble averaged persistent currents is also quite intriguing, and the calculations show that the disordered averaged current crucially depends on the choice of the ensemble^{27,29}. The explanation of experimental results become even much more illusive since recently Kravtsov *et al.*⁵⁸ have shown that additional currents may be generated in rings by other mechanisms which are not experimentally distinguishable from the persistent current.

A. Impurity free rings

To emphasize the precise role of electron-electron correlation, in this sub-section we focus on the exact calculation of persistent current and Drude weight in perfect

one-dimensional Hubbard rings⁵⁹ threaded by a magnetic flux ϕ . Our study reveals that, certain aspects of the many-body effects on persistent current have not been investigated in the literature clearly, and here we will show that the Hubbard correlation leads to many significant effects. We restrict ourselves to small Hubbard rings and these results might also be helpful to understand the physical properties of TTF-TCMQ conductors, various aromatic molecules and systems of connected quantum dots⁵⁵. With the new advancements of the nanoscience and technology, it is now possible quite simply to fabricate such small rings, and in a recent experiment Keyser *et al.*⁶⁰ reported the evidence of anomalous Aharonov-Bohm oscillations from the transport measurements on small quantum rings with less than ten electrons. The electron-electron interaction becomes much more important in these small rings with very few number of electrons since the Coulomb potential is not screened much, and we will show that the electron-electron interaction provides similar anomalous oscillations in persistent current as a function of magnetic flux ϕ .

We use the Hubbard model to represent the system which for a N -site ring enclosing a magnetic flux ϕ can be written in this form,

$$H = t \sum_{\sigma} \sum_{i=1}^N \left[e^{i\theta} c_{i,\sigma}^{\dagger} c_{i+1,\sigma} + e^{-i\theta} c_{i+1,\sigma}^{\dagger} c_{i,\sigma} \right] + U \sum_{i=1}^N n_{i\uparrow} n_{i\downarrow} \quad (15)$$

where $c_{i\sigma}^{\dagger}$ ($c_{i\sigma}$) is the creation (annihilation) operator and $n_{i\sigma}$ is the number operator for an electron in the Wannier state $|i\sigma\rangle$. The parameters t and U are the nearest-neighbor hopping integral and the strength of the Hubbard correlation, respectively. The phase factor $\theta = 2\pi\phi/N$ appears due to the flux ϕ threaded by the ring. Throughout this sub-section we set $t = -1$.

1. Persistent current and energy band structure

At absolute zero temperature ($T = 0\text{K}$), persistent current in a ring threaded by a magnetic flux ϕ is obtained through the expression²⁸,

$$I(\phi) = -\frac{\partial E_0(\phi)}{\partial \phi} \quad (16)$$

where, $E_0(\phi)$ is the ground state energy. We determine this quantity exactly to understand unambiguously the role of electron-electron interaction on persistent current, and this is obtained by exact numerical diagonalization of the many-body Hamiltonian (Eq. 15).

Rings with two opposite spin electrons: To have a deeper insight to the problem, we first consider two electron systems and begin our study with the simplest possible system which can be treated analytically up to certain

TABLE I: Eigenvalues (λ) and eigenstates of two opposite spin electrons for $N=3$.

Total spin S	$U = 0$		
	λ	Degeneracy	Eigenstate
0	-4	1	$\left(-\frac{1}{\sqrt{2}}, -\frac{1}{\sqrt{2}}, -\frac{1}{\sqrt{2}}, -1, -1, 1\right)$
	-1	2	$\left(0, \sqrt{2}, -\sqrt{2}, 1, 0, 1\right)$ $\left(-\sqrt{2}, 0, \sqrt{2}, -1, 1, 0\right)$
	2	3	$\left(\frac{1}{\sqrt{2}}, 0, \frac{1}{\sqrt{2}}, 0, 0, 1\right)$ $\left(0, -\frac{1}{\sqrt{2}}, -\frac{1}{\sqrt{2}}, 0, 1, 0\right)$ $\left(-\frac{1}{\sqrt{2}}, -\frac{1}{\sqrt{2}}, 0, 1, 0, 0\right)$
1	-1	2	$(1, 0, 1)$ $(-1, 1, 0)$
	2	1	$(-1, -1, 1)$

Total spin S	$U = 2$		
	λ	Degeneracy	Eigenstate
0	$-2\sqrt{3}$	1	$(a, a, a, -1, -1, 1)$
	0	2	$\left(0, \frac{1}{\sqrt{2}}, -\frac{1}{\sqrt{2}}, 1, 0, 1\right)$ $\left(-\frac{1}{\sqrt{2}}, 0, \frac{1}{\sqrt{2}}, -1, 1, 0\right)$
	3	2	$(0, -\sqrt{2}, \sqrt{2}, 1, 0, 1)$ $(\sqrt{2}, 0, -\sqrt{2}, -1, 1, 0)$
	$2\sqrt{3}$	1	$(b, b, b, -1, -1, 1)$
1	-1	2	$(1, 0, 1)$ $(-1, 1, 0)$
	2	1	$(-1, -1, 1)$

level. This is the case of a three-site ring with two opposite spin (\uparrow, \downarrow) electrons. The total Hamiltonian of this system becomes a (9×9) matrix which can be block diagonalized to two sub-matrices by proper choice of the basis states. The orders of the two sub-matrices are (6×6) and (3×3) , respectively. This can be achieved by constructing the basis states for each sub-space with a particular value of the total spin S . The basis set (\mathcal{A}) for the six-dimensional sub-space, spanned for $S = 0$, is chosen as:

$$\mathcal{A} \equiv \left\{ \begin{array}{l} |\uparrow\downarrow, 0, 0\rangle \\ |0, \uparrow\downarrow, 0\rangle \\ |0, 0, \uparrow\downarrow\rangle \\ \frac{1}{\sqrt{2}} (|\uparrow, \downarrow, 0\rangle - |\downarrow, \uparrow, 0\rangle) \\ \frac{1}{\sqrt{2}} (|0, \uparrow, \downarrow\rangle - |0, \downarrow, \uparrow\rangle) \\ \frac{1}{\sqrt{2}} (|\downarrow, 0, \uparrow\rangle - |\uparrow, 0, \downarrow\rangle) \end{array} \right\} \quad S = 0$$

On the other hand, the other basis set (\mathcal{B}) for the three-dimensional sub-space, spanned for $S = 1$, is chosen as:

$$\mathcal{B} \equiv \left\{ \begin{array}{l} \frac{1}{\sqrt{2}} (|\uparrow, \downarrow, 0\rangle + |\downarrow, \uparrow, 0\rangle) \\ \frac{1}{\sqrt{2}} (|0, \uparrow, \downarrow\rangle + |0, \downarrow, \uparrow\rangle) \\ \frac{1}{\sqrt{2}} (|\uparrow, 0, \downarrow\rangle + |\downarrow, 0, \uparrow\rangle) \end{array} \right\} \quad S = 1$$

In absence of any magnetic field, we list the energy eigen-

values, eigenstates, and the degeneracy of the levels of this system in Table I for $U = 0$ and $U = 2$. In this table we set $a = -\sqrt{2}/(1 + \sqrt{3})$ and $b = \sqrt{2}/(-1 + \sqrt{3})$. Both for $U = 0$ and $U \neq 0$ cases, the two-fold degeneracy gets lifted in the presence of magnetic flux ϕ . It is apparent from this table that the eigenvalues, eigenstates and also the degeneracy of the energy levels are not affected by the correlation in the three-dimensional sub-space. This is due to the fact that the basis set \mathcal{B} does not involve any doubly occupied state but this is not true in the other sub-space. The insertion of the magnetic flux does not alter the above structure of the Hamiltonian though it becomes now field dependent.

In Fig. 12(a), we show some of the low-lying energy levels $E(\phi)$'s as a function of magnetic flux ϕ of this three-site ring in absence of any electron correlation ($U = 0$),

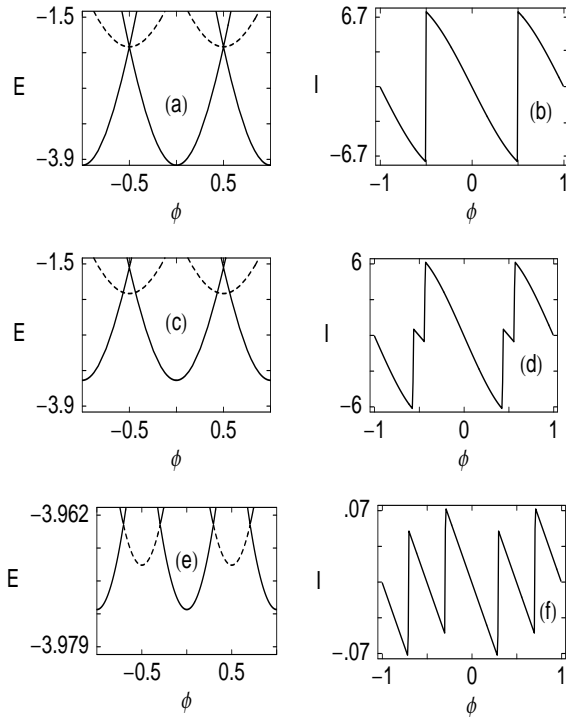


FIG. 12: E - ϕ and I - ϕ characteristics of the following two opposite spin (\uparrow, \downarrow) electron systems: (i) $N = 3$, $U = 0$ in (a) & (b); (ii) $N = 3$, $U = 2$ in (c) & (d); and (iii) $N = 25$, $U = 3$ in (e) & (f).

and the corresponding $I(\phi)$ versus ϕ curve is plotted in Fig. 12(b). The E - ϕ and I - ϕ curves for $U = 2$ case are given in Figs. 12(c) and (d), respectively. The dotted curves in Figs. 12(a) and (c) correspond to the U -independent energy levels as mentioned above. Quite interestingly, from Fig. 12(c) we see that even in presence of interaction, one of the U -independent energy levels becomes the ground state energy level in certain intervals of ϕ (e.g., around $\phi = \pm 0.5$). In other regions of ϕ , the ground state energy increases due to the correlation and the E_0 - ϕ curves become much shallower, as expected. As

a result, the usual saw-tooth shape of current-flux characteristics for $U = 0$ changes drastically as plotted in Fig. 12(d) and the role of e-e correlation is quite complex rather than a simple suppression of persistent current as predicted earlier. A sudden change in the direction and magnitude of persistent current occurs, solely due to the correlation, around $\phi = \pm 0.5$ and it forms kink-like structures in the current, as illustrated in Fig. 12(d). The kinks get wider with increasing the strength of U , and the most significant result is that the current remains invariant inside the kinks irrespective of the correlation strength. It is notice seen that, the correlation does not affect ϕ_0 flux periodicity of persistent current.

From this above background we can investigate the role of electronic correlation on persistent current in mesoscopic rings with larger sizes. In Figs. 12(e) and (f),

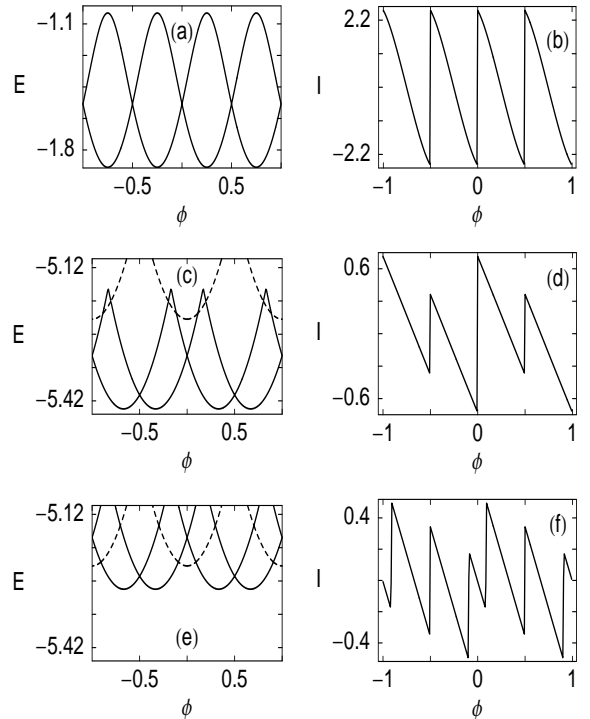


FIG. 13: E - ϕ and I - ϕ characteristics of the following three ($\uparrow, \uparrow, \downarrow$) electron systems: (i) $N = 3$, $U = 3$ in (a) & (b); (ii) $N = 10$, $U = 3$ in (c) & (d); and (iii) $N = 10$, $U = 15$ in (e) & (f).

we display E - ϕ and I - ϕ characteristics for the ring containing two opposite spin electrons with $N = 25$ and $U = 2$, respectively. These figures resemble Figs. 12(c) and (d), respectively, and it implies that correlation plays the same role in both the cases. Therefore, we can precisely conclude that away from half-filling, a ring consisting of two opposite spin electrons always exhibits kinks in persistent current for any non-zero value of U .

Rings with two up and one down spin electrons: Now we consider rings with two up and one down spin elec-

trons as illustrative examples of three spin electron systems. We plot the E - ϕ and I - ϕ curves for the half-filled band case ($N = 3$ and $n = 3$, where n denotes the number of electrons) with $U = 3$ in Figs. 13(a) and (b), respectively. We find that the correlation just diminishes the magnitude of the current compared to that of the non-interacting case. In Figs. 13(c) and (d), we respectively plot the E - ϕ and I - ϕ curves of a non-half-filled ring with $N = 10$ and $U = 3$, while Figs. 13(e) and (f) are these curves for the $U = 15$ case. The behavior of persistent current as a function of flux ϕ are quite different at low and high values of U . From Fig. 13(c), it is evident that for the low value of U all U -independent energy levels (dotted curves) always lie above the ground state energy

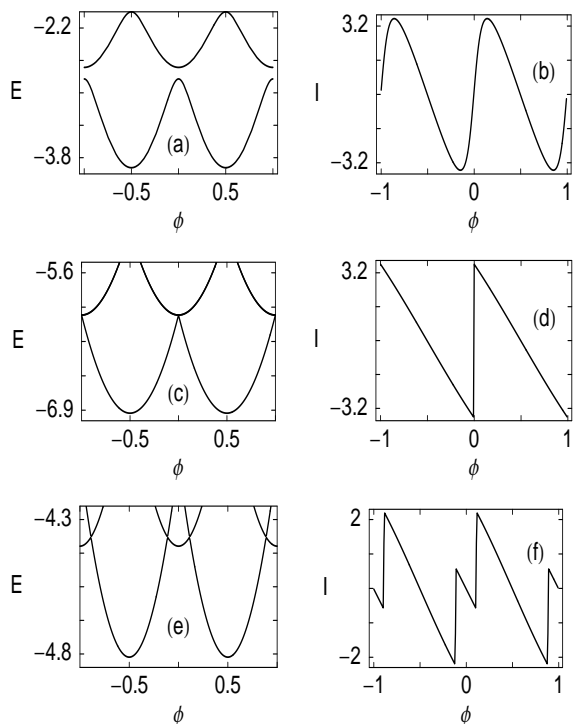


FIG. 14: E - ϕ and I - ϕ characteristics of the following four ($\uparrow, \uparrow, \downarrow, \downarrow$) electron systems: (i) $N = 4$, $U = 2$ in (a) & (b); (ii) $N = 6$, $U = 0$ in (c) & (d); and (iii) $N = 6$, $U = 6$ in (e) & (f).

of the system, and Fig. 13(d) shows that apart from a reduction of persistent current the I - ϕ curve looks very similar to that of a ring without any interaction. On the other hand, from Fig. 13(e) it is observed that for the high value of U one of the U -independent energy levels becomes the ground state energy in certain intervals of ϕ (e.g., around $\phi = 0$) and this produces kinks in the I - ϕ characteristics as depicted in Fig. 13(f). Certainly there exists a critical value U_c of the correlation above which the kinks appear in the I - ϕ characteristics. These features of the energy spectra and persistent currents are the characteristics of any non-half-filled ring with two up and one down spin interacting electrons. Here we note

that the half-filled rings exhibit $\phi_0/2$ periodic currents, while the non-half-filled rings have ϕ_0 periodicity.

Rings with two up and two down spin electrons: Next we consider rings with two up and two down spin electrons as representative examples of four electron system. Let us first describe the half-filled band case i.e., $N = 4$ and $n = 4$. In absence of any electron correlation, sharp discontinuity appears in persistent current at certain values of ϕ . However, the effect of the correlation is quite dramatic and it makes the current a continuous function of the flux as given in Fig. 14(b). This is a quite fascinating result since the correlation drastically changes

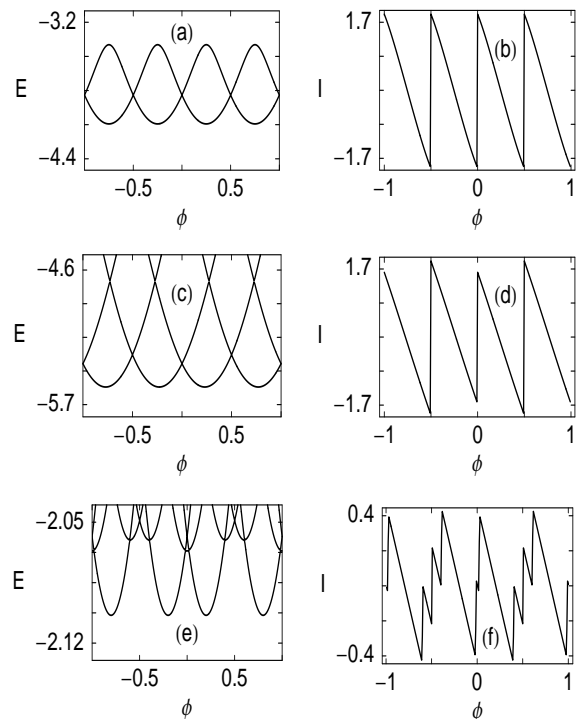


FIG. 15: E - ϕ and I - ϕ characteristics of the following five ($\uparrow, \uparrow, \uparrow, \downarrow, \downarrow$) electron systems: (i) $N = 5$, $U = 2$ in (a) & (b); (ii) $N = 6$, $U = 2$ in (c) & (d); and (iii) $N = 6$, $U = 120$ in (e) & (f).

the analytic behavior of $I(\phi)$, and here we will observe that this result also holds true for the other half-filled systems with even number of electrons. Away from the half-filling we study an interesting typical case of a six-site ring with two up and two down spin electrons. This can be considered as a doubly ionized benzene-like ring, a system with the promise of experimental verification of our predictions. Figures 14(c) and (d) show E - ϕ and I - ϕ characteristics with $U = 0$, respectively, while Figs. 14(e) and (f) are those plots with $U = 6$. It is observed from Fig. 14(f) that the kinks appear in the I - ϕ curve (e.g., around $\phi = 0$) for any non-zero value of U . Here we interestingly note that the kinks are now due to the U -dependent eigenstates. Both the half-filled and non-half-

filled rings exhibit ϕ_0 periodic currents.

Rings with three up and two down spin electrons: For specific cases of five electron systems we investigate rings with three up and two down spin electrons. In Figs. 15(a) and (b), we plot the E - ϕ and I - ϕ curves, respectively for the non-half-filled ring ($N = 5$ and $n = 5$). The magnitude of the current is just diminished due to e-e electron correlation and we find $\phi_0/2$ periodicity. As a non-half-filled five electron case, here we take a singly ionized benzene-like ring ($N = 6$ and $n = 5$) and determine the persistent current both for low and high values

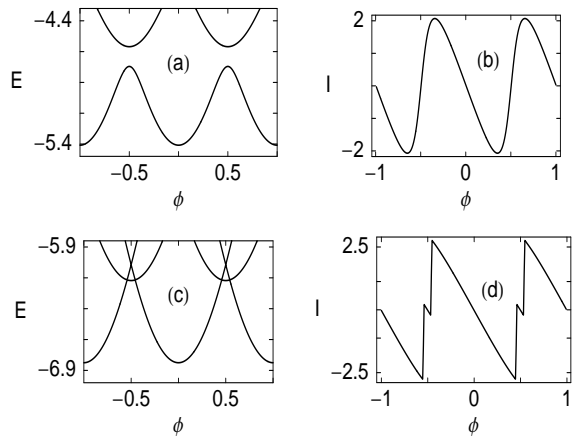


FIG. 16: E - ϕ and I - ϕ characteristics of the following six ($\uparrow, \uparrow, \uparrow, \downarrow, \downarrow, \downarrow$) electron systems: (i) $N = 6$, $U = 2$ in (a) & (b) and (ii) $N = 7$, $U = 2$ in (c) & (d).

of U . In Figs. 15(c) and (d), we respectively draw the E - ϕ and I - ϕ curves considering the correlation strength $U = 2$, while these diagrams are plotted in Figs. 15(e) and (f) with $U = 120$. From Figs. 15(d) and (f), it is clear that like three electron rings kinks appear in persistent current only after a critical value of U . This result emphasizes that the characteristic features of persistent current in mesoscopic Hubbard rings with odd number of electrons are almost invariant.

Rings with three up and three down spin electrons: Finally, we take six electron systems and study the nature of persistent current in rings with three up and three down spin electrons. At half-filling (a benzene-like ring with $N = 6$ and $n = 6$), we see that the current becomes a continuous function of flux ϕ as plotted in Fig. 16(b), exactly similar to the half-filled four electron case. The E - ϕ and I - ϕ curves for a typical non-half-filled ring with $N = 7$ and $n = 6$ are presented in Figs. 16(c) and (d), respectively. Here we find striking similarity in the behavior of persistent current with other non-half-filled systems containing even number of electrons. Therefore, it becomes apparent that mesoscopic Hubbard rings with even number of electrons exhibit similar characteristic features in persistent current.

2. Drude weight

In this sub-section we investigate the response of mesoscopic Hubbard rings to a uniform time-dependent electric field in terms of Drude weight^{61,62} D , a closely related parameter that characterizes the conducting nature of a system as originally predicted by Kohn⁶³. The Drude weight can be evaluated from the following expression⁵³,

$$D = \frac{N}{4\pi^2} \left[\frac{\partial^2 E_0(\phi)}{\partial \phi^2} \right]_{\phi=\phi_{\min}} \quad (17)$$

where, ϕ_{\min} provides the location of the minimum of energy $E_0(\phi)$. A metallic phase is characterized by a finite non-zero value of D , while it reaches to zero in an insulating phase⁶³. We show the variation of Drude weight D as a function of the Hubbard correlation strength U for the

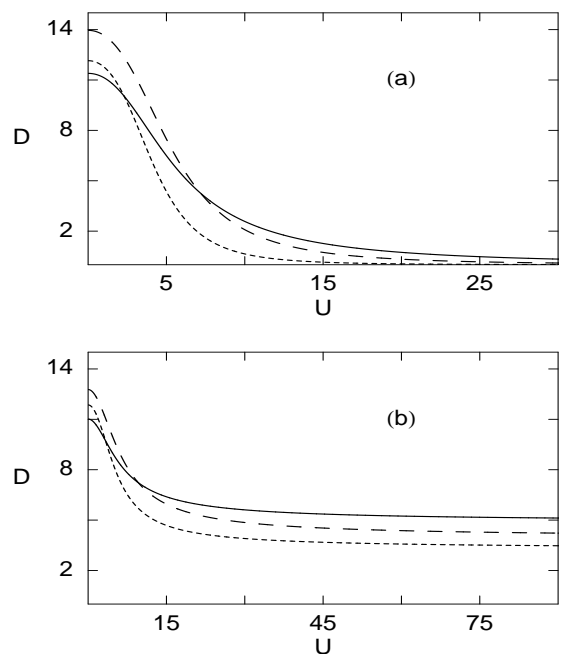


FIG. 17: Drude weight (D) versus the Hubbard correlation strength (U) for (a) half-filled and (b) non-half-filled band systems. The solid, dotted and dashed curves correspond to 3, 4 and 5 electron cases, respectively.

half-filled and non-half-filled rings with $n = 3, 4$ and 5 in Figs. 17(a) and (b), respectively. For the non-half-filled band cases, the number of sites corresponding to a given value of n is taken as $N = n + 1$, and we observe that the other choices of N do not affect the basic characteristics of the D - U curves. For low values of U , the half-filled systems are in the metallic phase which is clearly evident from Fig. 17(a), and the systems become insulating only when the correlation strength U becomes very large. In the insulating phase ground state does not favor any empty site, and accordingly, the situation is somewhat analogous to Mott localization in one-dimensional infinite lattices. On the other hand, Fig. 17(b) shows that

the non-half-filled rings are always conducting irrespective of the correlation strength U .

Throughout our analysis of persistent current in one-channel Hubbard rings without any impurity we get several interesting new results. The main results are: the appearance of kinks in persistent current, observation of both the ϕ_0 and $\phi_0/2$ periodicities in persistent current, no singular behavior of persistent current in the half-filled rings with even number of electrons, evidence of U -independent eigenstates, existence of both metallic and insulating phases, etc. We also observe discontinuities in persistent current at non-integer values of ϕ_0 due to the electron correlation which crucially depends on filling of the ring and also on the parity of the number of electrons. This corresponds to the anomalous Aharonov-Bohm oscillations in persistent current with much reduced period where periodicity is not perfect, and Keyser *et al.*⁶⁰ experimentally observed similar anomalous Aharonov-Bohm oscillations in conductance of a few-electron quantum ring.

B. Rings with impurities

To explore the role of disorder and electron-electron correlation on persistent current, in this sub-section we focus our attention on certain systems which closely resemble to the disordered systems where we do not require any configuration averaging⁶⁴. These are chemically modulated structures possessing well-defined long-range order and as specific examples we consider aperiodic and ordered binary alloy rings. We restrict ourselves to small one-dimensional rings, as in the previous sub-section, where persistent current can be calculated exactly. We get many interesting new results as a consequence of electron-electron interaction and disorder. One such promising result is the enhancement of persistent current amplitude in these systems due to the electronic correlation. This study might also be helpful to understand physical properties of benzene-like rings and other aromatic compounds in presence of magnetic flux ϕ .

1. Ordered binary alloy rings

Here we investigate current-flux characteristics in an ordered binary alloy ring (Fig. 18) at absolute zero temperature ($T = 0\text{K}$). A simple TB Hamiltonian is used to describe the system, and for a N -site ring it reads,

$$\begin{aligned}
 H = & \sum_{\sigma} \sum_{i=1,3,\dots}^{N-1} (\epsilon_A n_{i,\sigma} + \epsilon_B n_{i+1,\sigma}) \\
 & + t \sum_{\sigma} \sum_{i=1}^N \left(c_{i,\sigma}^{\dagger} c_{i+1,\sigma} e^{i\theta} + c_{i+1,\sigma}^{\dagger} c_{i,\sigma} e^{-i\theta} \right) \\
 & + U \sum_{i=1}^N n_{i\uparrow} n_{i\downarrow}
 \end{aligned} \tag{18}$$

where, ϵ_A and ϵ_B are the on-site potentials for the A and B type atoms. All the other symbols of this Hamiltonian carry the same meaning as described earlier. We always

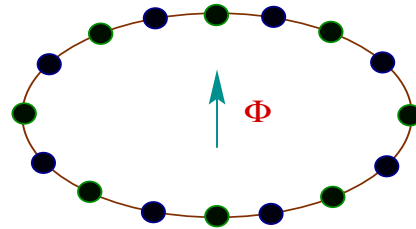


FIG. 18: (Color online). Schematic view of a one-dimensional tight-binding ordered binary alloy ring threaded by a magnetic flux ϕ . The green and blue circles correspond to two different types of atoms.

choose N to be even to preserve the perfect binary ordering of the two types of atoms in the ring, as shown in Fig. 18.

Let us now discuss the behavior of persistent current in an ordered binary alloy ring and investigate the role of electron-electron correlation on persistent current. In

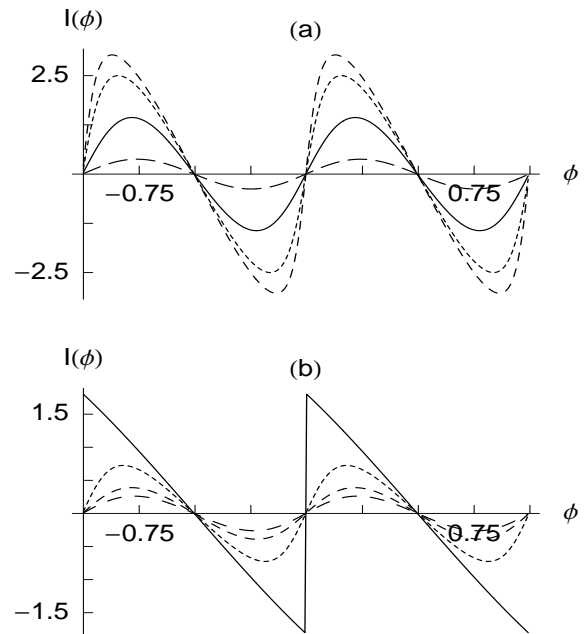


FIG. 19: Current-flux characteristics of four ($\uparrow, \uparrow, \downarrow, \downarrow$) electron ordered binary alloy rings, where (a) $N = 4$, $N_e = 4$ and (b) $N = 8$, $N_e = 4$. The solid, dotted, small dashed and dashed lines in (a) correspond to $U = 0, 2, 4$ and 10 , respectively, while in (b) they are for $U = 0, 2, 4$ and 6 , respectively.

a pure ring consisting of either A or B type of atoms and in absence of any electron correlation, the current shows discontinuity at certain points of ϕ due to ground state degeneracy and the I - ϕ curve gets a saw-tooth like be-

havior²⁸. This discontinuity completely disappears in a binary alloy ring with $U = 0$, as illustrated by the solid line in Fig. 19(a). This is due to the fact that, the binary alloy configuration may be considered as a perturbation over the pure ring which lifts the ground state degeneracy, and accordingly, the current $I(\phi)$ becomes a continuous function of magnetic flux. As we consider electron-electron interaction, current always decreases with the increase of interaction strength. However, depending on the number of electrons N_e in the ordered binary alloy rings, we get enhancement of persistent current for the low values of U , but it decreases eventually when U becomes very large. This type of behavior is depicted in Fig. 19(a), where we display the current-flux characteristics for a half-filled ordered binary alloy ring with four electrons (two up and two down spin electrons). We see that for $U = 2$ (dotted line) and $U = 4$ (small dashed line), current amplitudes are significantly larger than the non-interacting case, whereas for $U = 10$ (dashed line) the current amplitude becomes less than that from $U = 0$ case. This enhancement takes place above quarter-filling i.e., when $N_e > N/2$ and can be easily understood as follows. As N is even there are exactly $N/2$ number of sites with the lower site potential energy. If we do not take into account the electron-electron correlation, then above the quarter-filling it is preferred that some of these lower

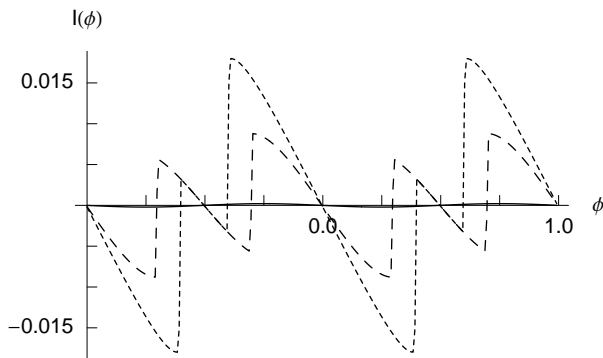


FIG. 20: Persistent current as a function of AB flux ϕ in a two (\uparrow, \downarrow) electron incommensurate ring, where the solid, dotted and dashed curves correspond to $U = 0, 1$ and 3 , respectively. The ring size N is fixed at 30 .

energy sites will be doubly occupied in the ground state. As we switch on the Hubbard correlation, the two electrons that are on the same site repel each other which results an enhancement in persistent current. But for large enough U , the hopping of the electrons is strongly suppressed by the interaction and the current amplitude gets reduced. On the other hand, at and below quarter-filling, no lower energy site will be doubly occupied in the ground state and hence there is no possibility of getting enhanced persistent current as a result of Coulomb repulsion. In these systems we always get the reduction of persistent current with increasing the strength U . In Fig. 19(b), we plot current-flux characteristics for a

quarter-filled binary-alloy ring with $U = 0, 2, 4$ and 6 , and it clearly noticed that persistent current is always suppressed due to this electronic correlation.

2. Rings with incommensurate site potentials

In this sub-section, we illustrate the behavior of persistent current in one-dimensional mesoscopic rings subject to quasi-periodic site potentials and study the effect of e-e interaction on persistent current. For a N -site ring with incommensurate site potentials, the TB Hamiltonian reads,

$$\begin{aligned}
 H = & \sum_{\sigma} \sum_{i=1}^N \epsilon \cos(i\lambda\pi) c_{i,\sigma}^{\dagger} c_{i,\sigma} \\
 & + t \sum_{\sigma} \sum_{i=1}^N \left(c_{i,\sigma}^{\dagger} c_{i+1,\sigma} e^{i\theta} + c_{i+1,\sigma}^{\dagger} c_{i,\sigma} e^{-i\theta} \right) \\
 & + U \sum_{i=1}^N n_{i\uparrow} n_{i\downarrow}
 \end{aligned} \tag{19}$$

where, λ is an irrational number and as a typical example we take it the golden mean, $\frac{1+\sqrt{5}}{2}$. For $\lambda = 0$, we get back the pure ring with identical site potential ϵ .

Rings with two opposite spin electrons: To investigate the precise role of electron-electron interaction on persistent current in presence of incommensurate site potentials let us first begin our discussion with a simplest possible system which is the case of a ring with two opposite spin (up and down) electrons. Figure 20 shows the current-flux characteristics of a 30-site incommensurate ring, where the solid, dotted and dashed lines correspond to $U = 0, 1$ and 3 , respectively. The current gets reduced significantly by the incommensurate site potentials in absence of any electron correlation. This is clearly observed from the solid line of Fig. 20, where it almost coincides with the abscissa. This is due to the fact that, in presence of aperiodic site potentials the electronic energy eigenstates are critical^{65,66} which tends to localize the electrons, and accordingly, the current amplitude gets decreased. But this situation changes quite dramatically as we include electron-electron interaction. From Fig. 20 it is clearly observed that the Hubbard correlation considerably enhances persistent current for the low values of U (dotted curve). The reason is that the repulsive Coulomb interaction does not allow double occupancy of the sites in the ground state and also it opposes the confinement of electrons as a result of localization. Therefore, the mobility of electrons increases as we introduce the electron-electron interaction and current gets enhanced. But such enhancement ceases to occur after certain values of U due to the ring geometry, and the current then decreases as we increase the correlation strength U further (dashed curve). Here we also observe that some strange kink-like structures appear in current-flux characteristics around

$\phi = \pm 0.5$ for finite values of U and inside these kinks persistent currents are independent of the Hubbard correlation strength. Therefore, it reveals that the kinks appear from the U -independent energy eigenstates of these rings. The explanation for the appearance of such kinks in persistent current has already been discussed in our previous sub-section for ordered rings. In these rings with

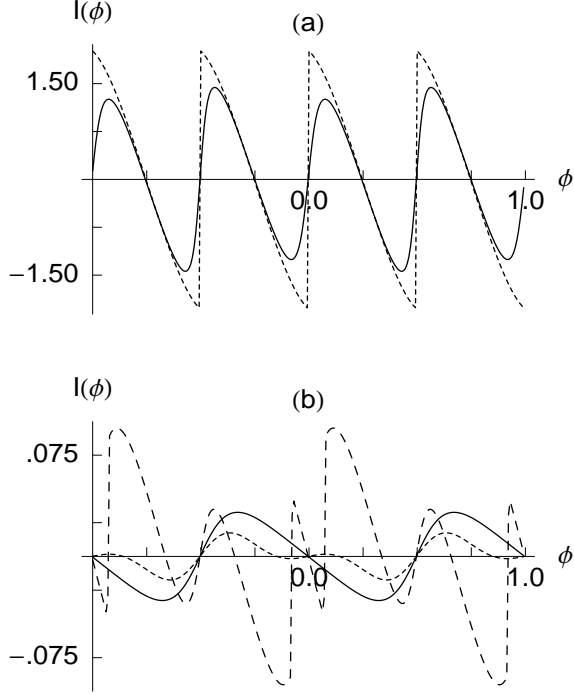


FIG. 21: Current-flux characteristics in a three ($\uparrow, \uparrow, \downarrow$) electron incommensurate ring. (a) Half-filled ring ($N = 3$) with $U = 4$, where the dotted and solid curves correspond to $\lambda = 0$ and $\lambda \neq 0$, respectively. (b) Non-half-filled ($N = 12$) ring with $\lambda \neq 0$, where the solid, dotted and dashed curves represent $U = 0, 4$ and 50 , respectively.

two opposite spin electrons, the current shows kink-like structures as long as the interaction is included, but in presence of the incommensurate site potentials kinks appear above some critical value of the correlation strength depending on the system size and strength of randomness. For such two-electron incommensurate rings we get ϕ_0 periodic currents.

Rings with two up and one down spin electrons: As representative examples of three-electron systems now we consider incommensurate rings with two up and one down spin electrons. In Fig. 21(a) we present current-flux characteristics for an half-filled ring ($N = 3$ and $N_e = 3$) when the correlation strength U is set at 4. The dotted curve of this spectrum corresponds to a pure ring ($\lambda = 0$) which exhibits discontinuous jumps at $\phi = 0, \pm 0.5$ due to the crossing of energy levels. Quite interestingly we observe that, this pure half-filled three-electron system ex-

hibits a perfect $\phi_0/2$ periodicity and we will see that this is a characteristic feature of pure half-filled rings with odd number of electrons. From the solid curve of this spectrum it is evident that, such $\phi_0/2$ periodicity no longer exists as we introduce the incommensurate site potentials and we get back the usual ϕ_0 flux-quantum periodicity. Moreover, in this case the current $I(\phi)$ becomes a continuous function with ϕ as the perturbation due to disorder lifts the ground state degeneracy at the crossing points

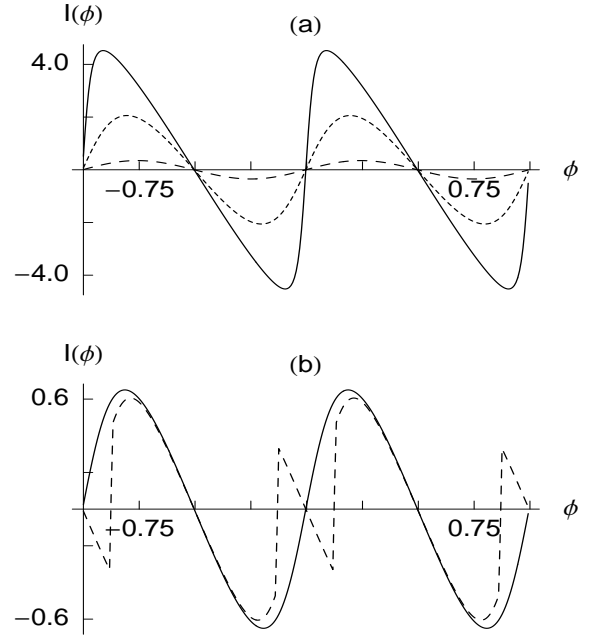


FIG. 22: Current-flux characteristics in a four ($\uparrow, \uparrow, \downarrow, \downarrow$) electron incommensurate ring. (a) Half-filled ($N = 4$) band case, where the solid, dotted and dashed lines correspond to $U = 0, 4$ and 10 , respectively. (b) Non-half-filled ($N = 8$) band case, where the solid and dashed lines are for $U = 4$ and 16 , respectively.

of the energy levels. The characteristic features of persistent current are quite different in the non-half-filled rings with two up and one down spin electrons. Figure 21(b) gives the results for a 12-site ring with incommensurate site potentials, where the solid, dotted and dashed lines represent $U = 0, 4$ and 50 , respectively. The role of the Hubbard correlation on persistent current in presence of the incommensurate site potentials becomes evident from these characteristics curves. For low values of U , the I - ϕ curve resembles to that for the non-interacting case and the current does not provide any discontinuity. But for large enough U , kink-like structures in persistent current are obtained as shown in Fig. 21(b) by the dashed curve. In this case also the kinks are due to the U -independent eigenstates like the two electron systems, and as explained earlier the currents inside the kinks become independent of the correlation strength U . It is observed that persistent currents always have ϕ_0 period-

icity in the non-half-filled systems. Here we also notice that for the half-filled systems, current always decreases with the increase of U , while in the non-half-filled rings current gets significant enhancement due to interplay between the electron correlation and the incommensurate site potentials.

Rings with two up and two down spin electrons: Next we address the characteristic features of persistent current in four-electron systems with incommensurate site potentials and as illustrative examples we consider rings with two up and two down spin electrons. In Fig. 22(a), we plot current-flux characteristics for an half-filled ring ($N = 4$ and $N_e = 4$), where the solid, dotted and dashed lines are for the cases with $U = 0, 4$ and 10 , respectively. From these curves it is clearly observed that the current

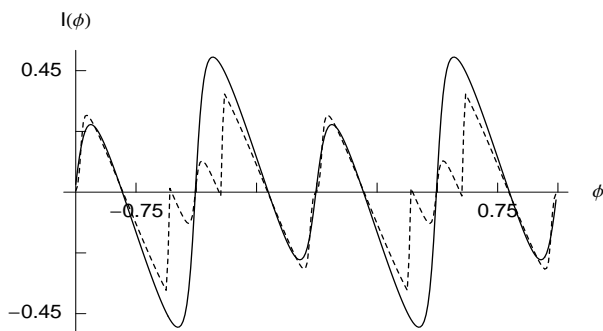


FIG. 23: Current-flux characteristics of a five ($\uparrow, \uparrow, \uparrow, \downarrow, \downarrow$) electron incommensurate ring away from the half-filled band case where the solid and dotted curves correspond to $U = 18$ and 120 , respectively. The ring size N is fixed at 7 .

amplitude gradually decreases with the increase of the correlation strength U . This reveals that in the half-filled case, electronic mobility gradually decreases with the increase of U , and we see that for large enough U , the system goes to an insulating phase. This kind of behavior holds true for any half-filled system, because at large enough U every site will be occupied by a single electron and the hopping of the electrons will not be favored due to strong electron-electron repulsion. Figure 22(b) displays the current-flux characteristics for a non-half-filled four-electron system with the aperiodic Harper potential. The solid and dotted curves are the I - ϕ curves for a 8-site ring with $U = 4$ and $U = 10$, respectively. This figure depicts that for low values of U , persistent current $I(\phi)$ has no discontinuity but kinks appear in the I - ϕ curve at large value of U . These kinks appear at sufficiently large value of U due to additional crossing of the ground state energy levels as we vary ϕ . It is important to note that, in the present case kinks appear due to the U -dependent states and not from the U -independent states as in the previous two- and three-electron cases. Both for the half-filled or non-half-filled incommensurate rings with four electrons, we observe that persistent current always exhibits ϕ_0 periodicity.

Rings with three up and two down spin electrons: Finally, we take five-electron aperiodic rings and evaluate persistent current in rings with three up and two down spin electrons. In a pure half-filled ring ($N = 5, N_e = 5$ and $\lambda = 0$), we get $\phi_0/2$ periodic persistent current and we have already observed such period halving in other pure half-filled systems with odd number of electrons (e.g., $N = 3, N_e = 3$ and $\lambda = 0$). Like the three-electron half-filled incommensurate rings, also in this case the ϕ_0 periodicity of the persistent current is restored once we introduce the incommensurate site potentials. The current-flux characteristics for the non-half-filled five-electron rings with $N = 7$ are shown in Fig. 23. The solid and dotted curves correspond to $U = 18$ and 120 , respectively. Similar to non-half-filled three-electron system, here also kinks appear in persistent current beyond a critical value of U . Another important observation is that for large U ($U = 120$), the maximum amplitude of the current remains finite. This is quite obvious since we consider the systems with $N > N_e$, where some sites become always empty so that electrons can hop to the empty sites which results the conducting phase. We also see that in these non-half-filled five-electron rings persistent currents always have the ϕ_0 periodicity.

Thus the analysis of persistent current in ordered binary alloy and aperiodic Hubbard rings yields many interesting results due to interplay between the electron-electron interaction and disorder in these systems. The significant results are: (a) In absence of electron correlation, the discontinuity in current-flux characteristics disappears due to disorder. This has been observed both in the ordered binary alloy rings and also in the aperiodic rings. (b) In pure rings with electron correlation, we observe both ϕ_0 and $\phi_0/2$ periodicities in persistent currents. However, in the incommensurate and ordered binary alloy rings persistent currents always have the ϕ_0 periodicity. (c) In ordered binary alloy rings, above the quarter-filling we get the enhancement of persistent current for small values of U and the current eventually decreases when U becomes large. On the other hand, at and below quarter-filling, persistent current always decreases with the increase of U . (d) An important finding is the appearance of kink-like structures in I - ϕ curves of the incommensurate rings only when we take into account the electron-electron interaction. Quite surprisingly we observe that, in some cases the currents inside the kinks are independent of the correlation strength U .

IV. ENHANCEMENT OF PERSISTENT CURRENT IN ONE-CHANNEL RINGS AND MULTI-CHANNEL CYLINDERS

Almost all the existing theories are basically based on the framework of nearest-neighbor TB model with either diagonal or off-diagonal disorder, and it has been observed that the simple nearest-neighbor TB Hamiltonian cannot explain the observed enhancement of per-

sistent current, even in presence of electron-electron interaction. In this sub-section, we will address the problem of the enhancement of persistent current in single-isolated-disordered mesoscopic one-channel rings and multi-channel cylinders, considering higher order hopping integrals in the Hamiltonian within a non-interacting electron picture, on the basis that the overlap of atomic orbitals between various neighboring sites are usually non-vanishing, and the higher order hopping integrals become quite significant^{67–69}. Physically, the higher order hopping integrals try to delocalize electrons even in one-dimension preserving their phase coherence and prevent the reduction of persistent current due to disorder. The fluctuations in persistent currents are also highly diminished due to the higher order hopping integrals. As a result, average amplitude of persistent current becomes comparable to I_0 and this is exactly what has been observed experimentally.

A. One-channel mesoscopic rings

We describe a N -site ring (Fig. 24) enclosing a magnetic flux ϕ (in units of the elementary flux quantum ϕ_0) by the following TB Hamiltonian in the Wannier basis,

$$H = \sum_i \epsilon_i c_i^\dagger c_i + \sum_{i \neq j} t_{ij} \left(c_i^\dagger c_j e^{i\theta_{ij}} + c_j^\dagger c_i e^{-i\theta_{ij}} \right) \quad (20)$$

where, ϵ_i is the on-site energy and the phase factor $\theta_{ij} = 2\pi\phi(|i-j|)/N$. Here we take the hopping integral between any two sites i and j through the expres-

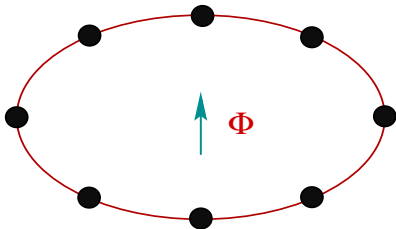


FIG. 24: (Color online). One-channel normal metal ring pierced by a magnetic flux ϕ . The filled circles correspond to the positions of the lattice sites.

sion $t_{ij} = t \exp[\alpha(1 - |i - j|)]$, where t corresponds to the nearest-neighbor hopping (NNH) strength. Since the hopping integrals between far enough sites give negligible contributions, we consider only one higher order hopping

integral in addition to the NNH integral which provides the hopping of an electron in the *next shortest path* between two sites. Therefore, in the case of strictly one-channel rings the next possible shortest path becomes the twice of the lattice spacing.

1. Impurity free rings

Here we concentrate on the behavior of persistent current both for impurity free mesoscopic rings described with only NNH integral, and rings described with

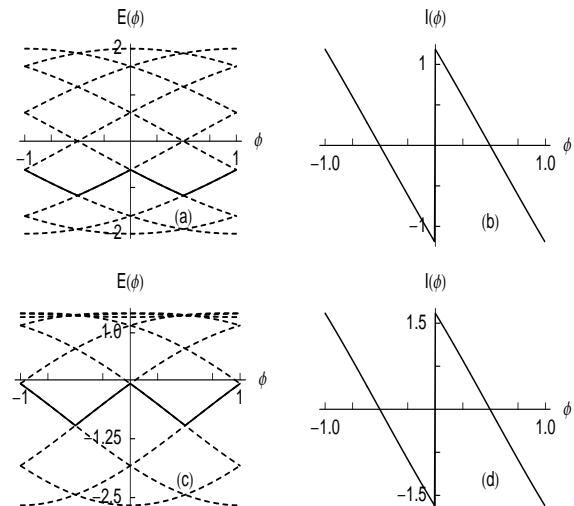


FIG. 25: Energy spectra and persistent currents of 10-site ordered rings with four electrons ($N_e = 4$), where (a) and (b) correspond to NNH model, while (c) and (d) correspond to SNH ($\alpha = 1.1$) model.

NNH integral in addition to the second-neighbor hopping (SNH) integral. In absence of any impurity, setting $\epsilon_i = 0$ in Eq. 20, the energy eigenvalue of the n th eigenstate can be expressed as,

$$E_n(\phi) = \sum_{p=1}^{p_0} 2t \exp[\alpha(1-p)] \cos \left[\frac{2\pi p}{N} (n + \phi) \right] \quad (21)$$

and the corresponding persistent current carried by this eigenstate becomes,

$$I_n(\phi) = \left(\frac{4\pi t}{N} \right) \sum_{p=1}^{p_0} \exp[\alpha(1-p)] \sin \left[\frac{2\pi p}{N} (n + \phi) \right] \quad (22)$$

where, p is an integer. We take $p_0 = 1$ and 2, respectively, for the rings with NNH and SNH integrals. For large values of α , the ring described with SNH integral eventually equivalent to the ring with only NNH integral. The contributions from the SNH integral become much more appreciable only when we decrease the value of α . In such case, the energy spectrum and the persistent current get modified and these modifications provide some interesting new results, which can be available from the following analysis.

To have a deeper insight to the problem, let us first describe the energy spectra and persistent currents of some small perfect rings ($N = 10$) containing four electrons ($N_e = 4$). The results are shown in Fig. 25. The energy

spectra for the rings described with NNH and SNH integrals are shown in Figs. 25(a) and (c), respectively. Here the solid curves represent the variation of the Fermi level at $T = 0\text{K}$ with flux ϕ . We see that the SNH integral lowers the energy levels, and most importantly, below the Fermi level the slopes of the $E(\phi)$ versus ϕ curves increases. As a result, the current gets increased in presence of SNH integrals and this enhancement of persistent current is clearly observed from Figs. 25(b) and (d). In Fig. 25, we have considered a 10-site ring only for the sake of illustration and the results for a larger ring are presented in Fig. 26.

In Fig. 26, we plot current-flux characteristics for some perfect rings with $N = 100$ and $\alpha = 0.9$. The dotted and solid curves correspond to the variation of persistent

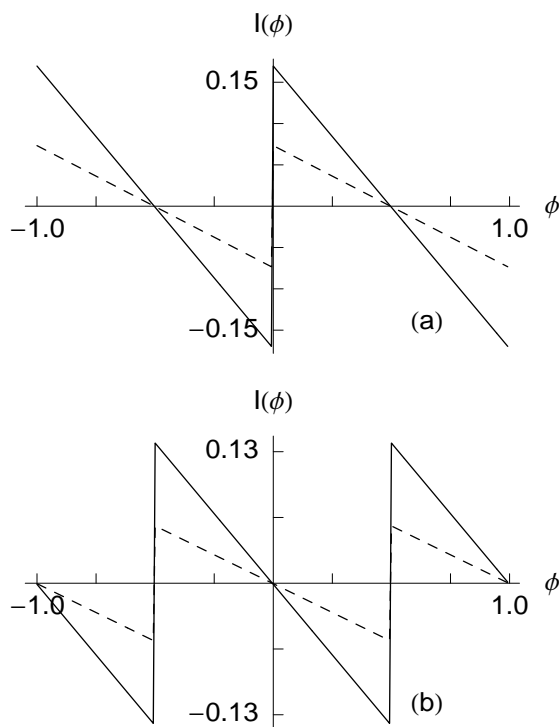


FIG. 26: Persistent current as a function of flux ϕ for some ordered rings with $N = 100$ and $\alpha = 0.9$, where (a) $N_e = 20$ and (b) $N_e = 15$. The dotted and solid curves correspond to the rings with NNH and SNH integrals, respectively.

current with flux ϕ for the rings described with NNH and SNH integrals, respectively. The enhancement of current amplitude due to the inclusion of SNH integral is clearly visible from Figs. 26(a) and (b) by comparing the results plotted by the dotted and the solid curves. Figure 26(a) shows that the current has sharp transitions at $\phi = 0$ or $\pm n\phi_0$, while in Fig. 26(b) the current shows transitions at $\phi = \pm n\phi_0/2$. These transitions are due to the degeneracy of energy eigenstates at these respective fields. For all the above models currents are always periodic in ϕ providing ϕ_0 flux-quantum periodicity.

2. Rings with impurity

In order to understand the role of higher order hopping integral on persistent current in disordered mesoscopic rings, we first describe the energy spectra and persistent currents in small rings. The results for a 10-site disor-

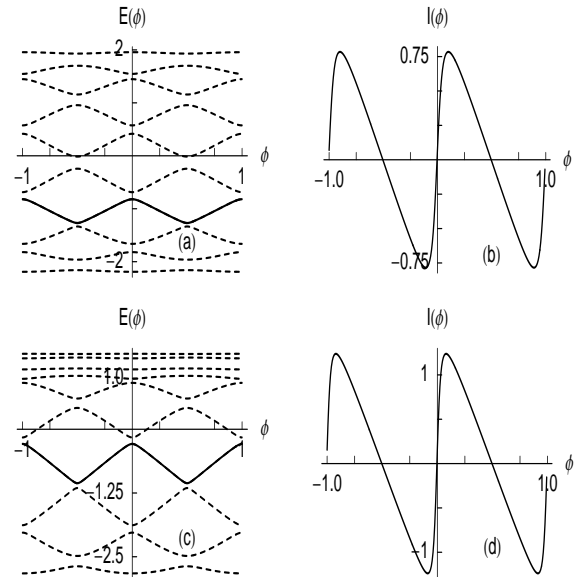


FIG. 27: Energy spectra and the persistent currents of 10-site disordered ($W = 1$) rings with four electrons ($N_e = 4$), where (a) and (b) correspond to NNH model, while (c) and (d) correspond to SNH ($\alpha = 1.1$) model.

dered ring with $N_e = 4$ are shown in Fig. 27. To describe the system we use the tight-binding Hamiltonian as given in Eq. 20, where the site energies (ϵ_i 's) are chosen randomly from a “Box” distribution function of width W . The energy spectra for the rings described with NNH and SNH integrals are plotted in Figs. 27(a) and (c), respectively. In these figures the solid curves give the location of the Fermi level. Like the ordered cases, the SNH integral lowers the energy levels and below the Fermi level slopes of the $E(\phi)$ versus ϕ curves become much more than those for the NNH model. Thus even in the presence of impurity, we get the enhancement of persistent current due to the SNH integral, which is observed from the results presented in Figs. 27(b) and (d), respectively.

In Fig. 28, we plot the current-flux characteristics for some larger disordered rings considering $N = 100$, $\alpha = 0.9$ and the disorder strength $W = 1$. The dotted and solid lines correspond to the rings described with NNH and SNH integrals, respectively. The results for the even number of electrons ($N_e = 20$) are shown in Fig. 28(a), while Fig. 28(b) represents the currents for the odd N_e ($N_e = 15$). The currents are computed for some typical disordered configurations of the ring, and in fact we observe that the qualitative nature of persistent current does not depend on the specific realization of the

disordered configurations. Figure 28 shows that persistent current for the disordered rings is always periodic in ϕ with ϕ_0 flux-quantum periodicity. In the presence of impurity, current becomes a continuous function of flux ϕ which is clearly visible from this figure (Fig. 28). For the perfect rings, sharp transitions in persistent current at the points $\phi = 0$ or $\pm n\phi_0$ with even N_e and at $\phi = \pm n\phi_0/2$ with odd N_e appear due to the degeneracy of the ground state energy at these respective field points. Now as the impurities are introduced, all the de-

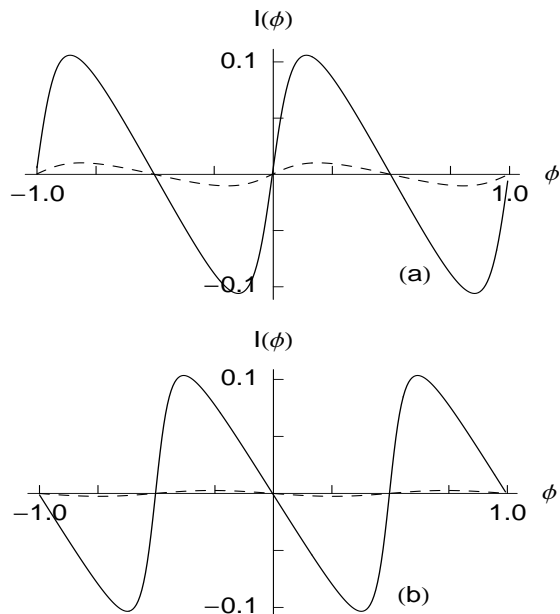


FIG. 28: Persistent current as a function of flux ϕ for some disordered rings with $N = 100$, $\alpha = 0.9$ and $W = 1$, where (a) $N_e = 20$ and (b) $N_e = 15$. The dotted and solid curves correspond to the rings with NNH and SNH integrals, respectively.

generacies get lifted and the current exhibits a continuous variation with respect to the flux ϕ . At these degenerate points, the ground state energy passes through an extrema which in turn gives the zero persistent current as shown in Fig. 28. It is clear from Fig. 28 that, the second-neighbor hopping (SNH) integral plays a significant role to enhance the amplitude of persistent current in disordered rings. From Figs. 28(a) and (b) we see that, the currents in disordered rings with only NNH integrals (dotted curves) are vanishingly small compared to those as observed in the impurity free rings with NNH integrals (dotted curves in Figs. 26(a) and (b)). On the other hand, Fig. 28 emphasizes that the currents in the disordered rings with higher order hopping integral are of the same order of magnitude as those for the ordered rings.

In Fig. 29, we plot persistent currents for some disordered rings with higher electron concentrations, and study the cases with $N =$ even or odd and $N_e =$ even or odd. The dotted and solid curves respectively corre-

sponds to the NNH and SNH models. It is observed that the evenness or the oddness of N and N_e do not play any important role on persistent current, but we will see later that the diamagnetic or the paramagnetic sign of the current crucially depends on the evenness or oddness of N_e .

Physically, the higher order hopping integrals try to delocalize electrons preserving their phase coherence and prevent the reduction of the current due to disorder. In disordered rings with only NNH integrals, the enormous

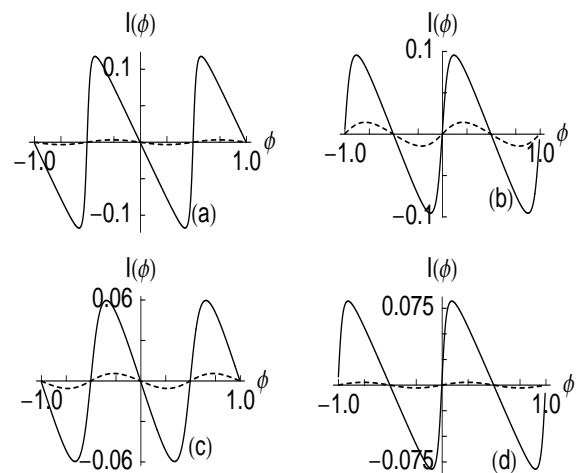


FIG. 29: Current-flux characteristics for some disordered rings with higher electron concentrations and we set $W = 1$ and $\alpha = 1.1$, where (a) $N = 125$, $N_e = 45$; (b) $N = 125$, $N_e = 40$; (c) $N = 150$, $N_e = 55$ and (d) $N = 150$, $N_e = 60$.

reduction of the current amplitudes are basically due to localization of the energy eigenstates. When we add higher order hopping integrals, it is most likely that the localization length increases and may become comparable to the length of the ring, and we get the enhancement of the persistent current.

B. Multi-channel mesoscopic cylinders

So far we have confined our discussions only to one-dimensional systems which do not really correspond to the experimental situations. Enhancement of the persistent current has been observed even in single-isolated diffusive (disordered) metallic rings. But diffusion is not possible strictly in one-dimension and it becomes necessary to consider finite width of the samples⁶⁹. The simplest way of doing this is to consider a cylindrical mesoscopic ring threaded by a magnetic flux ϕ . A schematic representation of the system is given in Fig. 30. Assuming that the lattice spacing both in the longitudinal and transverse directions are identical (i.e., surface of the cylinder forms a square lattice), we can describe the sys-

tem by the TB Hamiltonian as,

$$H = \sum_x \epsilon_x c_x^\dagger c_x + \sum_{\langle xx' \rangle} \left[t_{xx'} e^{i\theta_{xx'}} c_x^\dagger c_{x'} + t_{xx'} e^{-i\theta_{xx'}} c_{x'}^\dagger c_x \right] \quad (23)$$

where ϵ_x is the site energy of the lattice point x of coordinate, say, (i, j) . $t_{xx'}$ is the hopping integral between the lattice points x and x' and $\theta_{xx'}$ is the phase factor acquired by the electron due to this hopping in presence of magnetic flux ϕ . Let us now investigate the role of just the second-neighbor hopping integral on persistent current, and neglect the effects of all higher order hopping integrals. Let t denotes the nearest-neighbor hopping integral and the second-neighbor hopping integral (across

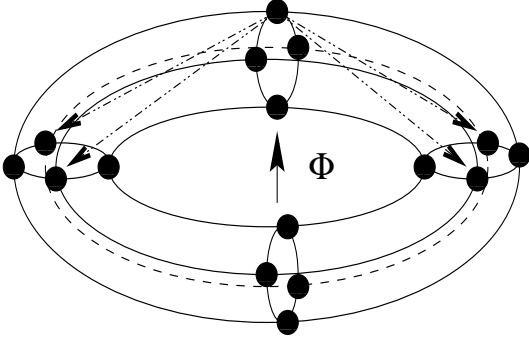


FIG. 30: Schematic view of a multi-channel mesoscopic cylinder threaded by a magnetic flux ϕ . The filled circles correspond to the positions of the lattice sites.

the diagonal of the square) is taken to have the exponential form: $t \exp(-\alpha)$, where α is the decay constant.

In absence of any impurity, setting $\epsilon_x = 0$, the energy eigenvalue of the n th eigenstate becomes,

$$E_n(\phi) = 2t \cos \left[\frac{2\pi}{N}(n + \phi) \right] + 4te^{-\alpha} \cos \left[\frac{2\pi}{N}(n + \phi) \right] \times \cos \left[\frac{2\pi m}{M} \right] + 2t \cos \left[\frac{2\pi m}{M} \right] \quad (24)$$

and the persistent current carried by this eigenstate is,

$$I_n(\phi) = \left(\frac{4\pi t}{N} \right) \sin \left[\frac{2\pi}{N}(n + \phi) \right] + \left(\frac{8\pi t}{N} \right) e^{-\alpha} \times \sin \left[\frac{2\pi}{N}(n + \phi) \right] \cos \left[\frac{2\pi m}{M} \right] \quad (25)$$

where, n and m are two integers bounded within the range $-[N/2] \leq n < [N/2]$ and $-[M/2] \leq m < [M/2]$, respectively, where $[\dots]$ denotes the integral part. Here M and N are the number of sites along the longitudinal and transverse directions of the cylinder, respectively.

Let us first describe the behavior of persistent current in a multi-channel cylinder using the nearest-neighbor tight-binding Hamiltonian. The results are shown in Fig. 31, where (a) and (b) correspond to $N_e = 45$ and 40, respectively. Here we set $N = 50$ and $M = 4$. The solid

curves describe the currents in absence of any impurity, while the dotted lines are for the disordered case and to introduce impurities ϵ_x 's are taken as random variables with uniform "Box" distribution of width W . The persistent current for the perfect cylinder (solid curves) has many discontinuities within each ϕ_0 flux-quantum period. These discontinuities are due to the existence

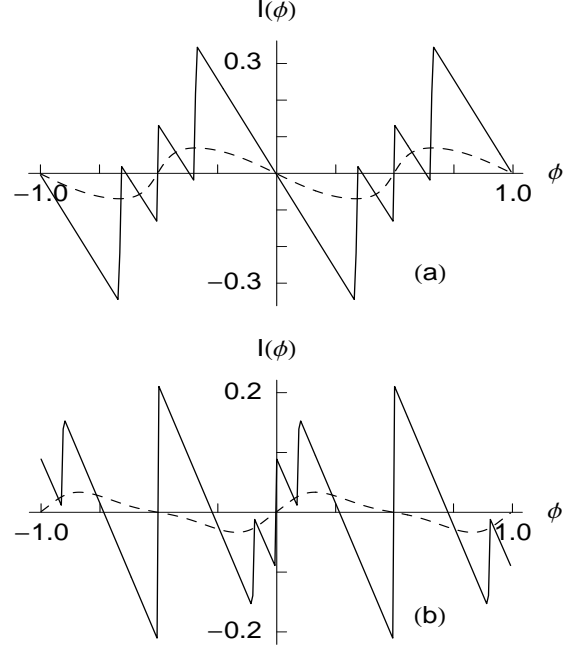


FIG. 31: Persistent current as a function of flux ϕ for a typical multi-channel mesoscopic cylinder with $N = 50$ and $M = 4$ described by NNH integral only, where (a) $N_e = 45$ and (b) $N_e = 40$. The solid and dotted lines are for the perfect ($W = 0$) and disordered ($W = 1$) cylinders, respectively.

of degenerate energy levels at certain magnetic flux, and these degeneracies get lifted as long as impurities are included. The current for the disordered system provides a continuous variation with ϕ as shown by the dotted lines in Figs. 31(a) and (b). It is observed that, even in multi-channel cylindrical systems the nearest-neighbor TB model gives orders of magnitude reduction of persistent currents compared to the results for the ballistic case.

The behavior of persistent current for the disordered mesoscopic cylinder changes drastically as we switch on the second-neighbor hopping integrals. In Fig. 32, we plot the current-flux characteristics for a multi-channel cylinder in presence of the second-neighbor hopping integral ($\alpha = 1$) considering $M = 50$ and $N = 4$. The results shown in Figs. 32(a) and (b) are respectively for the cylinders with $N_e = 45$ and 40, where the solid and dotted lines correspond to the identical meaning as in Fig. 31. From the spectra we see that the current amplitudes in the disordered cylinder (dotted curves) are comparable to that of the perfect systems (solid curves). This

is due to the fact that higher order hopping integrals try to delocalize the electrons, and accordingly, the current amplitudes get enhanced even by an order of magnitude in comparison with the estimates of current amplitudes in disordered cylinders using the nearest-neighbor TB Hamiltonian. This study reveals that for both the meso-

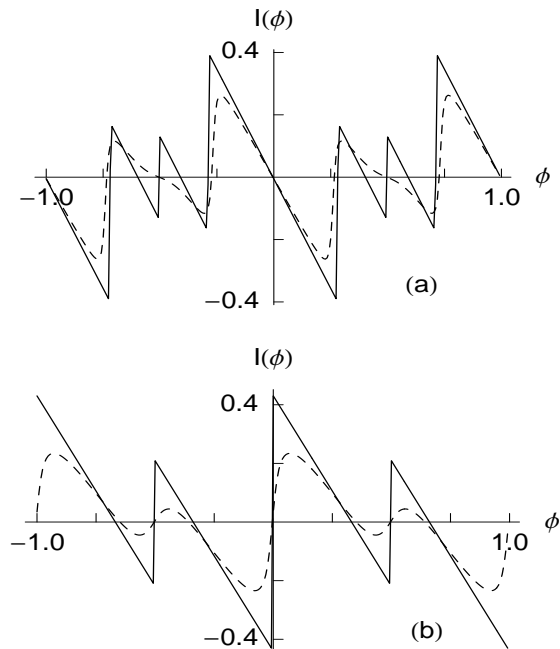


FIG. 32: Persistent current as a function of flux ϕ for a multi-channel mesoscopic cylinder described with both NNH and SNH ($\alpha = 1.0$) integrals, where (a) $N_e = 45$ and (b) $N_e = 40$. The solid and dotted curves correspond to the perfect ($W = 0$) and dirty ($W = 1$) cylinders, respectively. Here we fix $N = 50$ and $M = 4$.

scopic one-channel rings and the multi-channel cylinders the higher order hopping integrals play a very significant role in the enhancement of persistent current amplitude in disordered systems.

V. LOW-FIELD MAGNETIC RESPONSE ON PERSISTENT CURRENT

The diamagnetic or paramagnetic sign of low-field persistent currents also becomes a controversial issue due to discrepancy between theory and experiment. From the theoretical calculations, Cheung *et al.*²⁸ predicted that the sign of persistent current is random depending on total number of electrons, N_e , in the system and on specific realization of the disordered configurations of the ring. Both the diamagnetic and paramagnetic responses were also observed theoretically in mesoscopic Hubbard rings by Yu and Fowler⁵⁵. They showed that the rings with odd N_e exhibit paramagnetic response, while those with even N_e have diamagnetic response in the limit $\phi \rightarrow 0$.

In an experiment on 10^7 isolated mesoscopic Cu rings, Levy *et al.*¹⁸ had reported diamagnetic response for the low-field currents, while with Ag rings Chandrasekhar *et al.*²² got the paramagnetic phase. In a recent experiment, Jariwala *et al.*²¹ have got diamagnetic persistent currents with both integer and half-integer flux-quantum periodicities in an array of 30-diffusive mesoscopic gold rings. The diamagnetic sign of persistent currents in the vicinity of zero magnetic field were also found in an experiment¹⁹ on 10^5 disconnected Ag ring. The sign of the low-field current is a priori not consistent with the theoretical predictions. In this sub-section, we will study the nature of low-field magnetic response by calculating magnetic susceptibility of mesoscopic one-channel rings and multi-channel cylinders through some exact calculations.

The magnetic susceptibility of a N -site AB ring can be obtained from the general expression⁵⁶,

$$\chi(\phi) = \frac{N^3}{16\pi^2} \left[\frac{\partial I(\phi)}{\partial \phi} \right]. \quad (26)$$

Calculating the sign of $\chi(\phi)$, one can predict whether the current is paramagnetic or diamagnetic. Here we focus our attention on the systems either with fixed number of electrons N_e or with fixed chemical potential μ .

A. One-channel mesoscopic rings

Let us first analyze the behavior of low-field magnetic susceptibility in an impurity-free one-channel mesoscopic ring described with fixed N_e . Figure 33(a) shows the variation of $\chi(\phi)$ as a function of N_e for a perfect ring with $N = 200$ in the limit $\phi \rightarrow 0$. It is noticed that, both for the even and odd N_e , current has only the diamagnetic sign. This diamagnetic sign of the low-field currents can be easily understood from the slope of current-flux curve of one-channel impurity-free rings (see the curves given in Fig. 3). From these curves we observe that the current always exhibits negative slope at low-fields. Therefore, it can be predicted that for perfect one-channel rings current provides only the diamagnetic sign near zero-field limit, irrespective of the total number of electrons N_e i.e., whether the rings contain odd or even N_e .

The effects of disorder on low-field currents are quite interesting, and our results show that the sign of the currents, even in presence of disorder, can be mentioned without any ambiguity both for rings with odd and even N_e . In Fig. 33(b), we plot $\chi(\phi)$ as a function of N_e for the disordered case. Here we set $N = 200$ and $W = 1$. The solid and dotted lines correspond to the results for odd and even N_e , respectively. These curves show that the rings with odd N_e exhibit only the diamagnetic sign for the low-field currents, while for even N_e the low-field currents always have the paramagnetic sign. Physically, the disorder lifts all the degeneracies of the energy levels those were observed in a perfect ring, and as a result the sharp discontinuities of the I - ϕ curves (see the curves of Fig. 3) disappear. It may be noted that the slopes of

the I - ϕ curves for even and odd N_e always have opposite signs near zero magnetic field (see Fig. 6). Thus for one-dimensional disordered rings with fixed number of electrons, the sign of low-field current is independent of

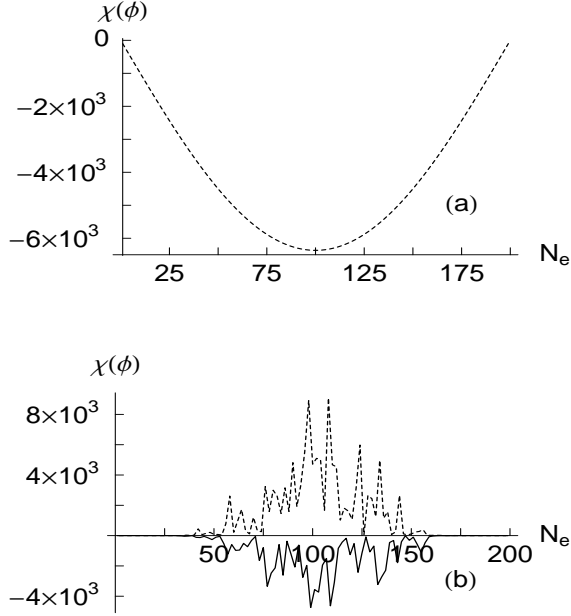


FIG. 33: Low-field magnetic susceptibility as a function of N_e for (a) perfect ring ($W = 0$) and (b) disordered ($W = 1$) ring. The solid and dotted lines in (b) correspond to the results for odd and even N_e , respectively. Here we set $N = 200$.

the specific realization of disordered configurations and depends only on the oddness or evenness of N_e .

Effect of temperature

At non-zero temperature, we notice an interesting behavior of low-field magnetic susceptibility in mesoscopic rings. Let us confine ourselves to the systems with even number of electrons. At any finite temperature, magnetic response of these systems are always paramagnetic both for perfect and disordered rings in the zero field limit. For a given system, this paramagnetism is observed over a certain range of ϕ close to $\phi = 0$, say, in the domain $\phi_0/4 \leq \phi \leq \phi_0/4$. Quite interestingly, we observe that, at finite temperatures the magnetic response of this particular system becomes diamagnetic beyond a critical field $\phi_c(T)$, even though $|\phi_c(T)| < \phi_0/4$.

In Fig. 34, we show the variation of the critical field $\phi_c(T)$ as a function of even N_e for a perfect 45-site one-channel ring. The curve with higher values of $\phi_c(T)$ corresponds to the temperature $T/T^* = 1.0$, while the other curve corresponds to $T/T^* = 0.5$. Figure 35, on the other hand, represents the behavior of $\phi_c(T)$ for a disordered sample (with $W = 1$) at the same temperatures, $T/T^* = 1.0$ (upper curve) and $T/T^* = 0.5$ (lower curve).

From these spectra (Figs. 34 and 35) it is clear that the critical value of ϕ , where the transition from the paramagnetic to diamagnetic phase takes place, increases with the increase of the temperature. Thus we see that, both for the perfect and disordered rings with even number

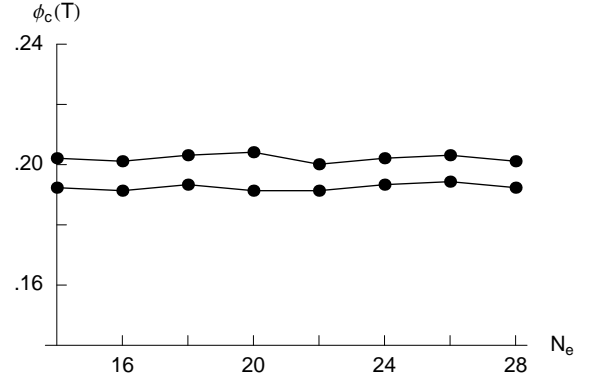


FIG. 34: $\phi_c(T)$ versus N_e (N_e =even) curves for perfect rings with size $N = 45$.

of electrons there exists a critical value of magnetic flux $\phi_c(T)$, beyond which the magnetic response of the low-

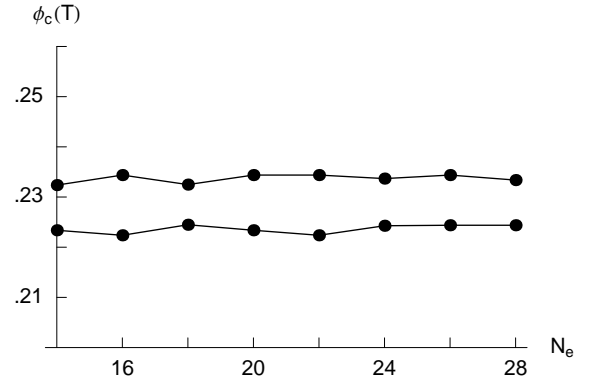


FIG. 35: $\phi_c(T)$ versus N_e (N_e =even) curves for disordered ($W = 1$) rings with size $N = 40$.

field currents exhibits a transition from the paramagnetic to the diamagnetic one.

The situation is quite different even at zero temperature when we describe the system by constant chemical potential instead of fixed N_e . It may be noted that, only for some particular values of μ the system will have a fixed number of electrons, and for these values of μ the sign of low-field currents can be predicted according to the above prescriptions. While, for all other choices of μ , total number of electrons varies even for a slight change in magnetic flux ϕ in the neighborhood of zero flux. Hence, it is not possible to predict the sign of the low-field currents precisely, even in absence of any impurity in the system. Thus the sign of low-field currents strongly depends on the choice of μ , strength of disorder and disordered configurations.

B. Multi-channel mesoscopic cylinders

We have also studied the low-field magnetic response in mesoscopic rings of finite widths⁵⁶. Our study reveals that, for such systems it is not possible to predict precisely the sign of the low-field currents even for impurity-free cases with fixed number of electrons. So we can conclude that, in diffusive multi-channel mesoscopic rings sign of the low-field currents is a highly unpredictable quantity as it can be easily affected by total number of electrons N_e , chemical potential μ , magnetic flux ϕ , strength of disorder W , realizations of disordered configurations, etc. This is exactly the same picture what has been observed experimentally regarding the sign of the low-field currents.

VI. CONCLUDING REMARKS

In the present review we have demonstrated quantum transport properties in different types of closed loop systems. These are one-channel rings, multi-channel cylinders, etc.

At the beginning of this review (Section I), we have described very briefly some of the spectacular effects those appear in mesoscopic systems as a consequence of the quantum phase coherence of electronic wave functions. One of the most remarkable consequences of the quantum phase coherence is the appearance of AB oscillations in normal metal mesoscopic rings. Some other mesoscopic phenomena that were observed in mesoscopic systems are the integer and fractional quantum Hall effects, conductance fluctuations and its quantization, etc. In this review, we have first concentrated on the spectacular mesoscopic phenomenon where a non-decaying current, the so-called persistent current, circulates in a small metallic loop threaded by a slowly varying magnetic flux. To understand the behavior of experimental results on persistent current, one has to focus attention on the interplay of quantum phase coherence, electron-electron correlation and disorder. This is a highly challenging problem and here we have tried to address this problem.

The characteristic features of persistent current in non-interacting single-channel rings and multi-channel cylinders have been presented in Section II showing its dependence on total number of electrons N_e , chemical potential μ , randomness and total number of channels. All the calculations have been performed only at absolute zero temperature. In perfect one-channel rings with fixed N_e , persistent current shows saw-tooth like behavior as a function of magnetic flux ϕ with sharp discontinuities at $\phi = \pm n\phi_0/2$ or $\pm n\phi_0$ depending on whether the ring contains odd or even N_e . On the other hand, some additional kinks may appear in persistent currents for one-channel perfect rings described with fixed μ . The situation is somewhat different for the multi-channel perfect cylinders. In such cylindrical rings, kinks appear in persistent currents for both the cases with fixed N_e or fixed μ .

In Section III, we have explored the effects of e-e correlation and disorder on persistent current in single-channel rings. We have used the TB Hubbard model and determine persistent current by exact numerical diagonalization of the Hamiltonian. First, we have studied the behavior of persistent current in some perfect small with few number of electrons. We have found many interesting results those are: the appearance of kinks in persistent current due to electron-electron interaction, existence of both $\phi_0/2$ and ϕ_0 flux-quantum periodicities in persistent current, disappearance of the singular behavior of persistent current in the half-filled rings with even number of electrons, existence of U -independent energy eigenstates, appearance of both the metallic and insulating phases, etc. The discontinuities in persistent current at non-integer values of ϕ_0 due to the electron correlation have also been observed, which crucially depend on the filling of the ring and also on the parity of the number of electrons. Next, we have investigated the effects of electron-electron correlation on persistent current in ordered binary alloy rings and aperiodic rings. The main results are: (a) In absence of electron correlation both for the ordered binary alloy and aperiodic rings the discontinuity in the I - ϕ curves disappears. (b) The persistent currents exhibit only ϕ_0 flux-quantum periodicity. (c) In ordered binary alloy rings with more than quarter-filled, we observe enhancement of persistent current for small values of U , but it eventually decreases when U becomes very large. On the other hand, at and below quarter-filling current always decreases with the strength of U .

Though we have noticed some enhancement of current amplitude in disordered rings due to Hubbard correlation, but still the amplitude is orders of magnitude smaller than the experimental estimates. In order to explain the enhancement of current amplitude, in Section IV we have calculated persistent currents in one-channel rings and multi-channel cylinders by inserting higher order hopping integrals together with nearest-neighbor hopping, within a non-interacting electron picture. The inclusion of the higher order hopping integrals is based on the fact that the overlap of atomic orbitals between various neighboring sites are usually non-vanishing, and these higher order hopping integrals try to delocalize electrons and prevent reduction of persistent current in presence of disorder. It has also been observed that the fluctuations of persistent currents are also significantly diminished due to the higher order hopping integrals and the results are comparable to the experimental values.

The diamagnetic or the paramagnetic sign of the low-field currents is a controversial issue due to the discrepancy between theory and experiment. At the end (Section V) of this review, we have examined the behavior of low-field magnetic response of persistent currents by calculating magnetic susceptibility in the limit $\phi \rightarrow 0$. In perfect one-channel rings, low-field current exhibits only the diamagnetic sign irrespective of the parity of the total number of electrons N_e i.e., whether N_e is odd or even, while in disordered rings currents have the diamag-

netic or the paramagnetic nature depending on whether the rings contain odd or even N_e . The important point is that, for disordered one-channel rings with fixed N_e the sign of the low-field currents is completely independent of the specific realization of the disordered configurations. In this context we have also studied the effect of finite temperature and observed that both for the perfect and disordered rings containing even number of electrons, there exists a critical value of magnetic flux $\phi_c(T)$ beyond which the magnetic response of the low-field currents makes a transition from the paramagnetic to diamagnetic phase. But in disordered rings described with fixed chemical potential μ , the sign of low-field currents cannot be predicted since it strongly depends on the choices of μ . Finally, in the case of multi-channel systems we have noticed that sign of these currents cannot be predicted exactly, even in the perfect case with fixed N_e as it significantly depends on the choice of N_e , μ , number of channels, disordered configurations, etc.

Future directions and opportunities: Although the

studies involving persistent currents in mesoscopic rings and cylinders have already generated a wealth of literature there is still need to look deeper into the problems both from the point of view of fundamental physics and to resolve a few issues that have not yet been answered in an uncontroversial manner. For example, it may be extremely interesting to study thermal signatures of persistent currents in metallic rings. The recent progress in the research on persistent currents in metallic rings suggests that by measuring heat capacity persistent current can be detected⁷⁰, and this approach is completely different from the conventional methods i.e., by measuring the ring's magnetic moment using a SQUID magnetometer^{18,21,22,24} or connecting the ring to a superconducting microresonator¹⁹, or by using a sophisticated micromechanical detector²⁵. The combined effect of electron-electron interaction and spin-orbit interaction on persistent current is also an interesting topic which should be carefully examined.

-
- * Electronic address: santanu.maiti@isical.ac.in
- ¹ S. Washburn and R. A. Webb, *Adv. Phys.* **35**, 375 (1986).
 - ² R. A. Webb and S. Washburn, *Physics Today* **41**, 46 (1988).
 - ³ K. von Klitzing, G. Dorda and M. Pepper, *Phys. Rev. Lett.* **45**, 494 (1980).
 - ⁴ R. E. Prange and S. M. Girvin. *The Quantum Hall Effect*. Springer-Verlag, New York (1987).
 - ⁵ T. Chakraborty and P. Pietiläinen. *The Quantum Hall Effects*. Solid-State Sciences. Springer, Berlin, second edition (1995).
 - ⁶ Y. Imry. *Introduction to Mesoscopic Physics*. Oxford University Press, New York (1997).
 - ⁷ D. C. Tsui, H. L. Stormer and A. C. Gossard, *Phys. Rev. Lett.* **48**, 1559 (1982).
 - ⁸ R. B. Laughlin, *Phys. Rev. Lett.* **50**, 1395 (1983).
 - ⁹ A. B. Fowler, A. Hartstein and R. A. Webb, *Phys. Rev. Lett.* **48**, 196 (1982).
 - ¹⁰ P. A. Lee, A. Douglas Stone and H. Fukuyama, *Phys. Rev. B* **35**, 1039 (1987).
 - ¹¹ D. Mailly, M. Sanquer, J.-L. Pichard and P. Pari, *Europhys. Lett.* **8**, 471 (1989).
 - ¹² B. J. van Wees, H. van Houten, C. W. J. Beenakker, J. G. Williamson, L. P. Kouwenhoven, D. van der Marel and C. T. Foxon, *Phys. Rev. Lett.* **60**, 848 (1988).
 - ¹³ D. A. Wharam, T. J. Thornton, R. Newbury, M. Pepper, H. Ahmed, J. E. F. Frost, D. G. Hasko, D. C. Peacock, D. A. Ritchie and G. A. C. Jones, *J. Phys. C: Solid State Phys.* **21**, L209 (1988).
 - ¹⁴ J. L. Costa-Krämer, N. Garcia, P. Garcia-Mochales and P. A. Serena, *Surf. Sci.* **342**, L1144 (1995).
 - ¹⁵ Y. Aharonov and D. Bohm, *Phys. Rev.* **115**, 485 (1959).
 - ¹⁶ F. Hund, *Ann. Phys. (Leipzig)* **32**, 102 (1938).
 - ¹⁷ M. Büttiker, Y. Imry and R. Landauer, *Phys. Lett. A* **96**, 365 (1983).
 - ¹⁸ L. P. Levy, G. Dolan, J. Dunsmuir and H. Bouchiat, *Phys. Rev. Lett.* **64**, 2074 (1990).
 - ¹⁹ R. Deblock, R. Bel, B. Reulet, H. Bouchiat and D. Mailly, *Phys. Rev. Lett.* **89**, 206803 (2002).
 - ²⁰ B. Reulet, M. Ramin, H. Bouchiat and D. Mailly, *Phys. Rev. Lett.* **75**, 124 (1995).
 - ²¹ E. M. Q. Jariwala, P. Mohanty, M. B. Ketchen and R. A. Webb, *Phys. Rev. Lett.* **86**, 1594 (2001).
 - ²² V. Chandrasekhar, R. A. Webb, M. J. Brady, M. B. Ketchen, W. J. Gallagher and A. Kleinsasser, *Phys. Rev. Lett.* **67**, 3578 (1991).
 - ²³ D. Mailly, C. Chapelier and A. Benoit, *Phys. Rev. Lett.* **70**, 2020 (1993).
 - ²⁴ H. Bluhm, N. C. Koshnick, J. A. Bert, M. E. Huber and K. A. Moler, *Phys. Rev. Lett.* **102**, 136802 (2009).
 - ²⁵ A. C. Bleszynski-Jayich, W. E. Shanks, B. Peaudecerf, E. Ginossar, F. von Oppen, L. Glazman and J. G. E. Harris, *Science* **326**, 272 (2009).
 - ²⁶ M. Büttiker, *Phys. Rev. B* **32**, 1846 (1985).
 - ²⁷ H.-F. Cheung, Y. Gefen, E. K. Riedel and W. H. Shih, *Phys. Rev. B* **37**, 6050 (1988).
 - ²⁸ H.-F. Cheung, E. K. Riedel and Y. Gefen, *Phys. Rev. Lett.* **62**, 587 (1989).
 - ²⁹ G. Montambaux, H. Bouchiat, D. Sigeti and R. Friesner, *Phys. Rev. B* **42**, 7647 (1990).
 - ³⁰ H. Bouchiat and G. Montambaux, *J. Phys. (Paris)* **50**, 2695 (1989).
 - ³¹ R. Landauer and M. Büttiker, *Phys. Rev. Lett.* **54**, 2049 (1985).
 - ³² N. Byers and C. N. Yang, *Phys. Rev. Lett.* **7**, 46 (1961).
 - ³³ F. von Oppen and E. K. Riedel, *Phys. Rev. Lett.* **66**, 84 (1991).
 - ³⁴ H. Bouchiat and G. Montambaux, *J. Phys. (Paris)* **50**, 2695 (1989).
 - ³⁵ B. L. Altshuler, Y. Gefen and Y. Imry, *Phys. Rev. Lett.* **66**, 88 (1991).
 - ³⁶ A. Schmid, *Phys. Rev. Lett.* **66**, 80 (1991).
 - ³⁷ M. Abraham and R. Berkovits, *Phys. Rev. Lett.* **70**, 1509 (1993).

- ³⁸ A. Müller-Groeling and H. A. Weidenmuller, *Phys. Rev. B* **49**, 4752 (1994).
- ³⁹ S. K. Maiti, *Solid State Phenomena* **155**, 87 (2009).
- ⁴⁰ S. K. Maiti, S. Saha, and S. N. Karmakar, *Eur. Phys. J. B* **79**, 209 (2011).
- ⁴¹ S. K. Maiti, *J. Appl. Phys.* **110**, 064306 (2011).
- ⁴² S. K. Maiti and A. Chakrabarti, *Phys. Rev. B* **82**, 184201 (2010).
- ⁴³ S. K. Maiti, *Solid State Commun.* **150**, 2212 (2010).
- ⁴⁴ S. K. Maiti, *Phys. Status Solidi B* **248**, 1933 (2011).
- ⁴⁵ S. K. Maiti, M. Dey, S. Sil, A. Chakrabarti, and S. N. Karmakar, *Europhys. Lett.* **95**, 57008 (2011).
- ⁴⁶ S. K. Maiti, *Nanotechnology Reviews* **1**, 255 (2012).
- ⁴⁷ V. Ambegaokar and U. Eckern, *Phys. Rev. Lett.* **65**, 381 (1990).
- ⁴⁸ V. Ambegaokar and U. Eckern, *Europhys. Lett.* **13**, 733 (1990).
- ⁴⁹ H. Bary-Soroker, O. Entin-Wohlman and Y. Imry, *Phys. Rev. Lett.* **101**, 057001 (2008).
- ⁵⁰ H. Bary-Soroker, O. Entin-Wohlman and Y. Imry, *Phys. Rev. B* **80**, 024509 (2009).
- ⁵¹ E. Ginossar, L. I. Glazman, T. Ojanen, F. von Oppen, W. E. Shanks, A. C. Bleszynski-Jayich and J. G. E. Harris, *Phys. Rev. B* **81**, 155448 (2010).
- ⁵² W. Rabaud, L. Saminadayar, D. Mailly, K. Hasselbach, A. Benoit and B. Etienne, *Phys. Rev. Lett.* **86**, 3124 (2001).
- ⁵³ G. Bouzerar, D. Poilblanc and G. Montambaux, *Phys. Rev. B* **49**, 8258 (1994).
- ⁵⁴ T. Giamarchi and B. S. Shastry, *Phys. Rev. B* **51**, 10915 (1995).
- ⁵⁵ N. Yu and M. Fowler, *Phys. Rev. B* **45**, 11795 (1992).
- ⁵⁶ S. K. Maiti, *Physica E* **31**, 117 (2006).
- ⁵⁷ P. A. Lee and T. V. Ramakrishnan, *Rev. Mod. Phys.* **57**, 287 (1985).
- ⁵⁸ V. E. Kravtsov and B. L. Altshuler, *Phys. Rev. Lett.* **84**, 3394 (2000).
- ⁵⁹ S. K. Maiti, J. Chowdhury and S. N. Karmakar, *Phys. Lett. A* **332**, 497 (2004).
- ⁶⁰ U. F. Keyser, C. Fühner, S. Borck and R. J. Haug, *Phys. Rev. Lett.* **90**, 196601 (2003).
- ⁶¹ D. J. Scalapino, R. M. Fye, M. J. Martins, J. Wagner and W. Hanke, *Phys. Rev. B* **44**, 6909 (1991).
- ⁶² D. J. Scalapino, S. R. White and S. Zhang, *Phys. Rev. B* **47**, 7995 (1993).
- ⁶³ W. Kohn, *Phys. Rev.* **133**, A171 (1964).
- ⁶⁴ S. K. Maiti, J. Chowdhury and S. N. Karmakar, *Solid State Commun.* **135**, 278 (2005).
- ⁶⁵ M. Kohmoto, B. Sutherland and C. Tang, *Phys. Rev. B* **35**, 1020 (1987).
- ⁶⁶ A. Chakrabarti, S. N. Karmakar and R. K. Moitra, *Phys. Lett. A* **168**, 301 (1992).
- ⁶⁷ S. K. Maiti, J. Chowdhury and S. N. Karmakar, *Synthetic Metals* **155**, 430 (2005).
- ⁶⁸ S. K. Maiti, *Int. J. Mod. Phys. B* **21**, 179 (2007).
- ⁶⁹ S. K. Maiti, J. Chowdhury and S. N. Karmakar, *J. Phys.: Condens Matter* **18**, 5349 (2006).
- ⁷⁰ G. M. Souche, J. Huillery, H. Pothier, P. Gandit, J. I. Mars, S. E. Skipetrov and O. Bourgeois, *Phys. Rev. B* **87**, 115120 (2013).